

---

# Brain-OF: An Omnifunctional Foundation Model for fMRI, EEG and MEG

---

Hanning Guo<sup>1,2</sup> Farah Abdellatif<sup>1,2</sup> Hanwen Bi<sup>3,4</sup> Andrei Galbenus<sup>1,2</sup> Jon. N. Shah<sup>1,5,6,7</sup> Abigail Morrison<sup>8,2</sup>  
Jürgen Dammers<sup>1,9</sup>

## Abstract

Brain foundation models have achieved remarkable advances across a wide range of neuroscience tasks. However, most existing models are limited to a single functional modality, restricting their ability to exploit complementary spatiotemporal dynamics and the collective data scale across imaging techniques. To address this limitation, we propose **Brain-OF**, the first omnifunctional brain foundation model jointly pretrained on fMRI, EEG and MEG, capable of handling both unimodal and multimodal inputs within a unified framework. To reconcile heterogeneous spatiotemporal resolutions, we introduce the *Any-Resolution Neural Signal Sampler*, which projects diverse brain signals into a shared semantic space. To further manage semantic shifts, the Brain-OF backbone integrates DINT attention with a Sparse Mixture of Experts, where shared experts capture modality-invariant representations and routed experts specialize in modality-specific semantics. Furthermore, we propose *Masked Temporal-Frequency Modeling*, a dual-domain pretraining objective that jointly reconstructs brain signals in both the time and frequency domains. Brain-OF is pretrained on a large-scale corpus comprising around 40 datasets and demonstrates superior performance across diverse downstream tasks, highlighting the benefits of joint multimodal integration and dual-domain pretraining.

## 1. Introduction

A central lesson from the recent success of deep learning is that pretraining on large-scale, high-quality and diverse data facilitates the emergence of general-purpose models that consistently outperform task-specific ones (Kaplan et al., 2020). Following this paradigm, brain foundation models have shown promising generalization across a wide range of neural signal processing tasks, including cognitive decoding, affective computing and neurological disease diagnosis (Jiang et al., 2024; Wang et al., 2024a; Dong et al., 2025). Despite this progress, the scale of available neuroimaging data remains orders of magnitude smaller than the billion-scale corpora in natural language processing and computer vision. Although open-source large-scale neuroimaging collections are growing, data from any single modality remain scarce for training large models due to high acquisition costs and privacy constraints. Meanwhile, most existing brain foundation models are pretrained on a single modality, restricting both data scale and representational diversity, and failing to exploit the complementary characteristics of different brain signals. To address these limitations, we integrate data from the three primary functional neuroimaging modalities (fMRI, EEG and MEG) to develop an *omnifunctional* brain foundation model.

A pivotal question, therefore, is how to effectively leverage such heterogeneous multi-modal data to pretrain an omnifunctional brain foundation model. The first challenge lies in the variability introduced by diverse scanning devices, sampling rates, acquisition protocols and recording durations across international sites, leading to significant **structural variability**. A deeper challenge stems from the fundamental differences in the physical imaging mechanisms of each modality. Specifically, fMRI detects hemodynamic changes, such as oxygenation, blood volume and flow, to measure the Blood-Oxygen-Level-Dependent (BOLD) signal, offering high spatial resolution but limited temporal fidelity (Logothetis & Pfeuffer, 2004). In contrast, EEG captures electrical potentials generated by cortical neurons, providing excellent temporal resolution but poor spatial fidelity (He et al., 2018). MEG records magnetic fields induced by neuronal electrical activity and shares EEG’s high temporal resolution while providing improved spatial localization, though still inferior to that of fMRI (Wheless et al., 2004). These distinct

---

<sup>1</sup>INM-4, Forschungszentrum Jülich, Germany <sup>2</sup>Department of Computer Science 3 - Software Engineering, RWTH Aachen University, Germany <sup>3</sup>INM-7, Forschungszentrum Jülich, Germany <sup>4</sup>Institute of Systems Neuroscience, Heinrich Heine University, Germany <sup>5</sup>Department of Neurology, RWTH Aachen University, Germany <sup>6</sup>JARA-BRAIN-Translational Medicine, Germany <sup>7</sup>INM-11, JARA, Forschungszentrum Jülich, Germany <sup>8</sup>IAS-6, Forschungszentrum Jülich, Germany <sup>9</sup>Department of Psychiatry, Psychotherapy and Psychosomatics, RWTH Aachen University, Germany. Correspondence to: Jürgen Dammers <j.dammers@fz-juelich.de>.

Preprint. March 2, 2026.

signal origins result in severe differences in spatiotemporal resolution and **semantic heterogeneity**. However, this heterogeneity also presents a unique opportunity. By integrating these modalities, a unified model can exploit the high temporal resolution of EEG and MEG to compensate for the temporal latency of fMRI, while leveraging the superior spatial specificity of fMRI to resolve ambiguities in electrophysiological sources. Such complementary integration enables a holistic characterization of temporal, spectral, and spatial dynamics, ultimately fostering richer and more transferable representations. A third challenge is the inherently low signal-to-noise ratio of brain signals, which can mislead vanilla attention mechanisms to attend to irrelevant fluctuations rather than biologically meaningful patterns.

On the other hand, the success of large-scale pretraining is fundamentally rooted in the generative learning paradigm, which insists that reconstruction compels models to internalize the underlying data distribution (Radford et al., 2018; Han et al., 2021). Brain signals are inherently multidimensional, characterized by complex spatial configurations, rich temporal dynamics and structured frequency compositions. Although recent brain foundation models have introduced dual-branch architectures to jointly process temporal and spectral features (Wang et al., 2024a; Zhou et al., 2025), frequency domain information is typically treated as a static auxiliary input for passive feature extraction, rather than as a target for active reconstruction. Therefore, a specialized pretraining objective is essential to explicitly enforce joint reconstruction across both temporal and frequency domains. By coupling temporal and spectral reconstruction, the model is compelled to capture complementary dynamics and intrinsic semantics of neural signals across heterogeneous modalities.

To address these challenges, we propose **Brain-OF**, an omnifunctional brain foundation model designed to learn holistic representations from neural signals across the three primary functional modalities: fMRI, EEG and MEG. Our architecture integrates a Sparse Mixture of Experts (MoE) with DINT attention to effectively model heterogeneous semantic tokens generated by the Any-Resolution Neural Signal Sampler (ARNESS), which projects signals of varying spatiotemporal resolutions into a unified semantic space. The main contributions are summarized as follows:

- **Unified Omnifunctional Framework.** We introduce Brain-OF, a unified framework capable of processing both unimodal and multimodal brain data within a single model. We curate a large-scale corpus comprising over 40 publicly available datasets across fMRI, EEG and MEG. To the best of our knowledge, Brain-OF is the first brain foundation model to integrate these three modalities, enhancing generalization across modalities, tasks, sites and subjects.
- **Heterogeneity Aligned Architecture.** We propose

ARNESS to project heterogeneous neural signals into a shared semantic space. To accommodate semantic diversity, we employ a Sparse MoE architecture in which shared experts capture modality-invariant features while routed experts specialize in modality-specific semantics. Furthermore, we incorporate DINT attention to suppress irrelevant context and efficiently capture both local and global dependencies.

- **Joint Time-Frequency Pretraining.** We introduce Masked Temporal-Frequency Modeling (MTFM), a novel pretraining objective that enforces the joint reconstruction of original signals in both the time and frequency domains. This dual-domain paradigm enables the model to internalize complementary physical dynamics of brain activity, leveraging the high temporal resolution of EEG/MEG to compensate for the latency of fMRI and vice versa.

## 2. Related Work

**Brain Foundation Models.** Foundation models have significantly advanced brain AI by learning generalizable representations from large-scale neuroimaging data. In fMRI, pioneering works such as BrainLM (Caro et al., 2023) and BrainMass (Yang et al., 2024) employ self-supervised learning to model BOLD time series. Subsequent approaches like Brain-JEPA (Dong et al., 2024) further advanced this direction by employing joint-embedding predictive architectures to improve spatiotemporal representation learning. Parallel advancements in EEG have led to models such as BENDR (Kostas et al., 2021), MMM (Yi et al., 2023) and BrainBERT (Wang et al., 2023), which demonstrated the efficacy of contrastive and masked modeling objectives for capturing temporal dynamics in EEG signals. Recently, LaBraM (Jiang et al., 2024) and CbraMod (Wang et al., 2024a) have utilized massive data to enhance general-purpose EEG representation learning. Despite these advances, those foundation models remain confined to single modalities, failing to leverage the complementary characteristics across functional neuroimaging modalities.

**Heterogeneous Foundation Models.** More recently, a growing line of work has begun to address heterogeneity by jointly modeling multiple signal types within unified foundation frameworks. BIOT (Yang et al., 2023a) pioneered this direction by pretraining on biosignals, specifically EEG and ECG. Within the electrophysiological domain, PopT (Chau et al., 2025) learns joint representations across variable channel configurations for both intracranial and scalp EEG, while BrainOmni (Xiao et al., 2025) extends to jointly model EEG and MEG signals. Beyond purely electrophysiological modalities, BrainHarmonix (Dong et al., 2025) bridges structural and functional neuroimaging by combining fMRI and MRI. Similarly, PhysioOmni (Jiang et al., 2025a) decouples homogeneous and heterogeneous features across multimodal physiological signals, including EEG,

ECG, EOG and EMG. However, these approaches fall short of capturing the full spectrum of brain activity, missing the opportunity to harmonize the high spatial fidelity of hemodynamic signals with the high temporal resolution of electromagnetic fields. This gap motivates a unified framework for integrating heterogeneous brain signals across fundamentally different physical measurement principles.

### 3. Method

In this work, we propose **Brain-OF**, a heterogeneous pre-training framework (Figure 1) designed as a unified brain foundation model that supports both unimodal and multimodal data. The framework is explicitly designed to achieve broad generalization across four key dimensions: *cross-modality*, *cross-task*, *cross-site* and *cross-subject* settings. To address the intrinsic heterogeneity of brain signals, Brain-OF introduces an *Any-Resolution Neural Signal Sampler*, which projects inputs with diverse spatial, temporal, and spectral resolutions into a shared semantic space. To further model heterogeneous semantics while mitigating the allocation of attention to irrelevant context, the backbone integrates *DINT attention* with a *Sparse Mixture of Experts*. Finally, to learn informative representations, we propose *Masked Temporal-Frequency Modeling*, which jointly captures complementary knowledge in both the temporal and frequency domains.

#### 3.1. Model Architecture

In this section, the set of modalities is defined as  $\mathcal{M} = \{M_{\text{fMRI}}, M_{\text{EEG}}, M_{\text{MEG}}\}$ . For any given modality  $M_i \in \mathcal{M}$ , the normalized brain signal is represented as a matrix  $S \in \mathbb{R}^{N \times T}$ , where  $N$  denotes the number of channels (for M/EEG) or regions of interest (ROIs; for fMRI), and  $T$  represents the temporal length of the signal.

**Brain Signal Encoder.** The primary challenge in handling our heterogeneous corpus, spanning diverse modalities, sites, tasks and devices, is the **structural variability** in channel/ROI counts  $N$  and temporal lengths  $T$ . To standardize the normalized brain signal  $S$ , we adopt a patching and flattening strategy using a fixed time window  $\mathcal{T}$ . Specifically,  $S$  is segmented into non-overlapping patches of length  $\mathcal{T}$  along the temporal dimension for each channel/ROI, then flattened into a consistent sequence  $X_c \in \mathbb{R}^{L \times \mathcal{T}}$ , where  $L = N \cdot \lceil \frac{T}{\mathcal{T}} \rceil + \text{padding tokens}$ . The sequence is padded to a maximum length of 2,048 to ensure uniform input across modalities. Each patch in  $X_c$  is subsequently processed by a temporal encoder comprising stacked 1D convolutional layers to capture local temporal dynamics, followed by RMSNorm and GELU activation. This yields a sequence of patch embeddings  $X \in \mathbb{R}^{L \times D}$ , where  $D$  is the embedding dimension:

$$X = \{x_{\text{patch}_1}, x_{\text{patch}_2}, \dots, x_{\text{patch}_{N \cdot \lceil T/\mathcal{T} \rceil}}, \dots, x_{\text{padding}_L}\}$$

An attention mask is generated to exclude zero-padded patches from attention computations, eliminating spurious interactions and ensuring training stability.

**Any-Resolution Neural Signal Sampler.** Despite the structural unification of the input into sequence  $X$ , intrinsic differences in temporal, spatial and spectral resolutions persist across modalities, resulting in significant **semantic heterogeneity**. To bridge this gap and enable a single model backbone to efficiently process diverse unimodal or multimodal signals, we introduce the **Any-Resolution Neural Signal Sampler (ARNESS)**. As illustrated in Figure 1b, ARNESS employs Perceiver-style cross-attention (Alayrac et al., 2022) to project the heterogeneous sequence  $X$  into a shared semantic space via a fixed number of learnable latent tokens  $Z \in \mathbb{R}^{C \times D}$  ( $C = 128$  in our implementation). Specifically,  $X$  and  $Z$  are concatenated to form the Keys and Values, with  $Z$  serving as the Queries in cross-attention, thereby resampling essential semantic information from the high-dimensional  $X$  into a compact, fixed-length  $Z$ :

$$\text{ARNESS}(X, Z) = \text{CrossAttn}(Q = Z, KV = [X; Z], \text{Attn\_Mask})$$

This approach enables the subsequent backbone to handle all inputs uniformly, despite inherent heterogeneity. Lower-resolution modalities can potentially benefit by preserving the meaningful semantic space shaped by higher-resolution modalities. It also dramatically reduces the number of tokens for high-dimension brain signals, significantly lowering pretraining computational costs.

Moreover, ARNESS naturally supports multimodal fusion (Figure 1c) by sequentially resampling multiple unimodal sequences into a single fixed-length representation **without requiring modality-specific fusion branches**:

$$Z^{(i+1)} = \text{ARNESS}(X^{(i)}, Z^{(i)}), \quad i \in \mathcal{M}$$

**DINT Attention Mechanism.** The vanilla self-attention mechanism often overallocates attention to irrelevant context, resulting in "attention noise." This issue is particularly detrimental in neuroimaging, where residual noise in pre-processed brain signals can exacerbate this phenomenon, leading to coarse attention patterns and degraded performance (Guo et al., 2025). To mitigate this, we introduce the **Differential-Integral (DINT) Attention mechanism** (Cang et al., 2025), which extends Differential Attention (Ye et al., 2024) to capture precise local dependencies while amplifying global relevance and suppressing noise in the semantic space  $Z$ .

The differential component reduces noise by computing the difference between two attention distributions. The query and key projections from  $Z$  are split into halves,  $(Q_1, Q_2)$  and  $(K_1, K_2)$ , respectively. The differential attention matrix  $A_{\text{diff}}$  is defined as:

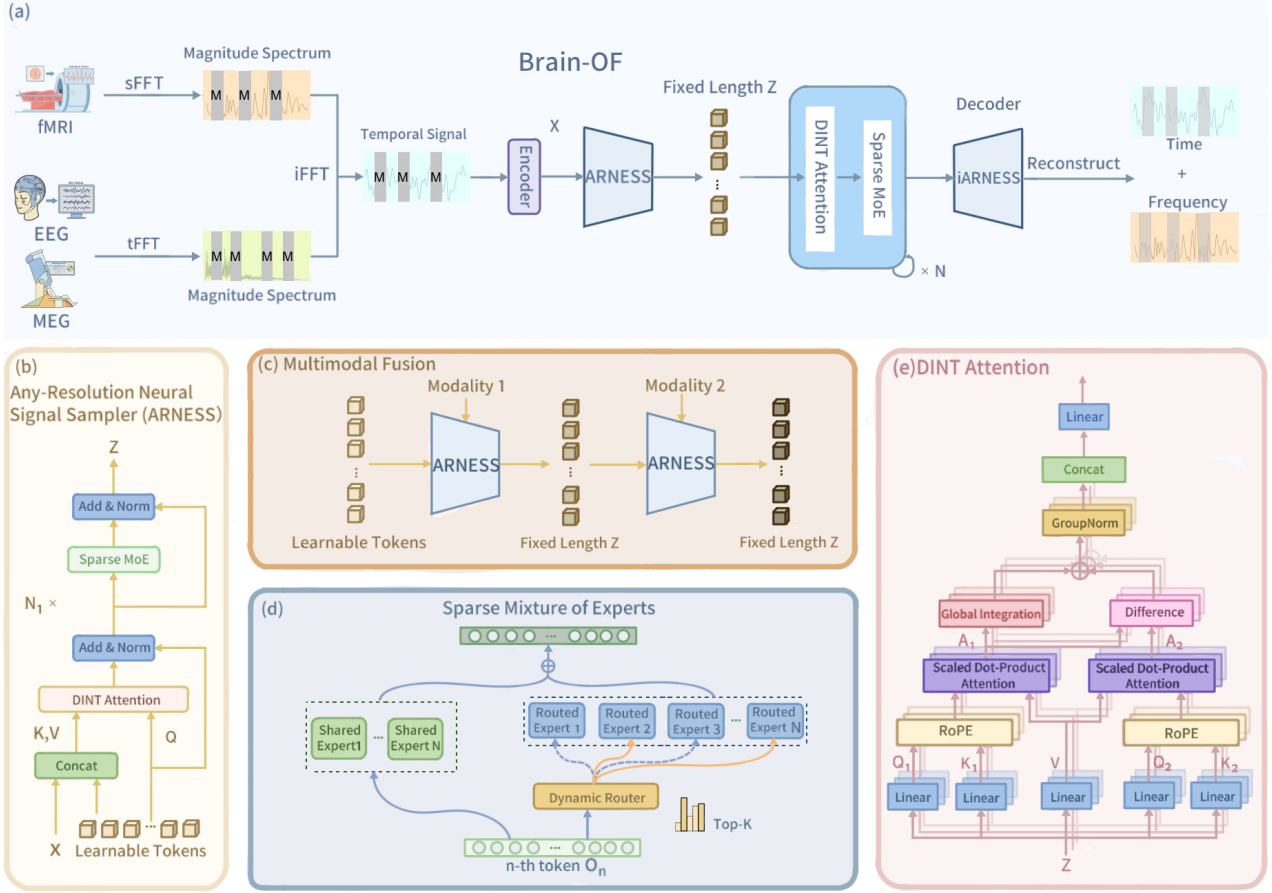


**Figure 1. Overview of the Brain-OF Architecture.** Brain-OF is an omnifunctional foundation model jointly pretrained on fMRI, EEG and MEG. **(a) Pretraining pipeline:** The original signals are masked in both the temporal and frequency domains to encourage the model to jointly learn coupled time–frequency representations. **(b) ARNESS** projects arbitrary resolution signals into a unified semantic space and also serves as a decoder to inverse-sample latent representations for reconstruction during pretraining. **(c) Multimodal Fusion** serially resamples multiple unimodal sequences via ARNESS without introducing modality-specific fusion branches. **(d) Sparse MoE** addresses semantic heterogeneity by dynamically routing tokens to specialized experts while extracting modality-invariant knowledge through shared experts. **(e) DINT Attention** mitigates attention allocation to irrelevant contextual information. Here, sFFT and tFFT denote Fast Fourier Transform along spatial and temporal dimensions; iFFT denotes the inverse Fast Fourier Transform; and  $M$  indicates the masking.

$$A_{\text{diff}} = \text{softmax} \left( \frac{Q_1 K_1^\top}{\sqrt{d}} \right) - \lambda \cdot \text{softmax} \left( \frac{Q_2 K_2^\top}{\sqrt{d}} \right)$$

where the learnable scalar  $\lambda$  is reparameterized as  $\lambda = \exp(\lambda_{q_1} \cdot \lambda_{k_1}) - \exp(\lambda_{q_2} \cdot \lambda_{k_2}) + \lambda_{\text{init}}$ .  $\lambda_{\text{init}}$  is a constant initialization value and  $\lambda_{q,k}$  are learnable parameters. Following empirical settings (Ye et al., 2024), we set  $\lambda_{\text{init}} = 0.8 - 0.6 \cdot \exp(-0.3 \cdot (l - 1))$ , where  $l$  denotes the layer depth.

To capture global dependencies, the integral component computes a global importance score by averaging the columns of the first attention map  $A_1$  (from  $Q_1, K_1$ ):

$$G = \frac{1}{C} \sum_{i=1}^C A_1[i, j]$$

yielding  $G \in \mathbb{R}^{1 \times C}$ . To align dimensions for combination,  $G$  is expanded along the query dimension to form

$G_{\text{expanded}} \in \mathbb{R}^{C \times C}$ . The final output integrates local (differential) and global (integral) semantics:

$$\text{DINTAttn}(Z) = (A_{\text{diff}} + \lambda \cdot G_{\text{expanded}}) V$$

In addition,  $G_{\text{expanded}}$  ensures row sums of one, guaranteeing numerical stability. Rotary Position Embeddings (RoPE) (Su et al., 2024) are used in our model to encode relative positional information within the sequence.

**Sparse Mixture of Experts.** Our preliminary experiments using dense feedforward layers revealed a *modality seesaw* effect, where improvements for one modality (e.g., fMRI) degraded performance for others (EEG/MEG). This arises from the diverse semantic features of fMRI, EEG and MEG within the sequence  $Z$ . To address this, we adopt a **Sparse Mixture of Experts (SMoE)** architecture, which excels at modeling heterogeneous semantic spaces. Specifically, we employ a combination of shared experts for modality-invariant representations and routed experts for

Table 1. Overview of downstream tasks and evaluation datasets.

Downstream Tasks	Datasets	Modalities	#Channels/ROIs	Durations	#Participants	#Samples	Labels
Emotion Recognition	SEED-V	EEG	62	1s	20	117,744	5-class
Seizure Detection	CHB-MIT	EEG	22	10s	22	326,993	2-class
Abnormal Detection	TUAB	EEG	19	10s	2,383	409,455	2-class
AD Diagnosis	ADNI	fMRI	246	~300s	222	618	2-class
ADHD Identification	ADHD-200	fMRI	246	~360s	926	1,369	2-class
Brain Age Prediction	CamCAN	fMRI	246	520s	652	652	regression
	CamCAN	MEG	306	2s	643	177,044	regression
	CamCAN	MEG + fMRI	-	-	621	171,057	regression
Aging Classification	LEMON	fMRI	246	448s	219	438	2-class
	LEMON	EEG	61	10s	203	17,235	2-class
	LEMON	EEG + fMRI	-	-	194	16,471	2-class

modality-specific information. Each expert is implemented via a Feed-Forward Network (FFN). For the  $n$ -th token  $O_n$  from the DINT attention output, the SMoE layer is defined as:

$$\text{SMoE}(O_n) = O_n + \sum_{i=1}^{N_s} \text{FFN}_i^{(s)}(O_n) + \sum_{i \in \mathcal{I}_n} g_{i,n} \text{FFN}_i^{(r)}(O_n)$$

where  $N_s$  is the number of shared experts, and  $\mathcal{I}_n$  denotes the indices of the top- $k$  routed experts selected for token  $O_n$ . The routing weights  $g_{i,n}$  are normalized over the selected routed experts:

$$g_{i,n} = \frac{p_{i,n}}{\sum_{j \in \mathcal{I}_n} p_{j,n}}$$

where  $p_{i,n}$  is the raw probability generated by a sigmoid-activated gating network. To prevent expert collapse, we use an auxiliary-loss-free load-balancing strategy (Wang et al., 2024b). A bias term  $b_i$  is added to  $p_{i,n}$  prior to top- $k$  selection (i.e., selection is based on  $p_{i,n} + b_i$ ), while the actual routing weights for aggregating routed experts rely solely on  $p_{i,n}$ . At the end of each training step,  $b_i$  is dynamically adjusted by a bias update rate  $\gamma$ : decreased for overloaded experts and increased for underloaded ones. Through the dynamic adjustment, SMoE keeps balanced expert load without additional auxiliary losses.

### 3.2. Pretraining

**Masked Temporal-Frequency Modeling (MTFM).** The efficacy of foundation models stems largely from self-supervised pretraining, which facilitates the learning of rich representations by reconstructing masked inputs to capture underlying data distributions. In neuroimaging, brain signals inherently contain complementary information in both the temporal, spatial and frequency domains. Consequently, effective representation learning requires a model to internalize coupled features from both spectral and temporal perspectives. To achieve this, we introduce **Masked Temporal-Frequency Modeling (MTFM)** for learning informative representations across temporal and frequency domains in all modalities. Given a normalized timecourse of a brain signal  $S$ , we first transform it into its frequency

domain representation  $F_S$ . Due to the distinct characteristics of different modalities, richer spatial information in fMRI and higher temporal resolution in EEG and MEG, we apply modality-specific frequency transformations:

$$F_S = \begin{cases} \mathcal{F}_{\text{spatial}}(S), & \text{if } S \in M_{\text{fMRI}} \\ \mathcal{F}_{\text{temporal}}(S), & \text{if } S \in \{M_{\text{EEG}}, M_{\text{MEG}}\} \end{cases}$$

where  $\mathcal{F}$  denotes the Fourier transform applied along the spatial dimension for fMRI or the temporal dimension for EEG and MEG. Here, the spatial FFT over ROIs is not intended to model physical spatial frequencies, but serves as a fixed orthogonal transform to encourage global cross-region structure learning. Within the frequency domain, we apply a random frequency mask  $M_F$ , with a masking ratio sampled from a normal distribution. The masked frequency representation is then transformed back to the original signal domain via the inverse Fourier transform. To further enhance temporal modeling, a second masking operation  $M_T$  is applied to randomly occlude temporal patches in this spectrally perturbed signal. Following the backbone, a lightweight one-layer ARNESS decoder inverse-samples the latent representations to reconstruct the signal. The model is pretrained to jointly reconstruct both the masked temporal patches and the frequency components, thereby fostering the learning of coupled time-frequency representations.

**Loss Function.** The pretraining objective combines reconstruction losses in both the temporal and frequency domains:

$$\mathcal{L}_{\text{MTFM}} = (1 - \alpha) \cdot \mathcal{L}_{\text{SL1}}(\hat{S}, S) + \alpha \cdot \mathcal{L}_{\text{SL1}}(|\hat{F}_S|, |F_S|)$$

where  $\hat{S}$  denotes the reconstructed signal and  $\hat{F}_S = \mathcal{F}(\hat{S})$  is its frequency domain representation;  $|\cdot|$  indicates the magnitude; and  $\alpha = 0.8$  is empirically chosen to balance the temporal and frequency reconstruction terms. We utilize the smooth L1 loss ( $\mathcal{L}_{\text{SL1}}$ ) to ensure stable optimization and robustness to outliers.

## 4. Experiments

### 4.1. Datasets

**Pre-training.** We curate a heterogeneous collection of **37 public neuroimaging datasets** to jointly pretrain Brain-OF

Table 2. Comparison results of different methods on downstream tasks.

Methods	SEED-V	CHB-MIT	TUAB	ADNI	ADHD-200	CamCAN	CamCAN	LEMON	LEMON
	EEG	EEG	EEG	fMRI	fMRI	fMRI	MEG	fMRI	EEG
	Kappa(%) $\uparrow$	BAC(%) $\uparrow$	BAC(%) $\uparrow$	BAC(%) $\uparrow$	BAC(%) $\uparrow$	MAE $\downarrow$	MAE $\downarrow$	BAC(%) $\uparrow$	BAC(%) $\uparrow$
ContraWR	19.05 $\pm$ 1.88	63.44 $\pm$ 0.02	77.46 $\pm$ 0.41	59.69 $\pm$ 4.97	62.67 $\pm$ 1.69	9.15 $\pm$ 0.39	9.01 $\pm$ 0.40	63.97 $\pm$ 1.28	77.42 $\pm$ 0.45
CNN-Transformer	20.72 $\pm$ 1.83	63.89 $\pm$ 0.67	77.77 $\pm$ 0.22	62.27 $\pm$ 4.87	61.94 $\pm$ 0.43	16.00 $\pm$ 0.10	15.69 $\pm$ 0.09	<b>64.83<math>\pm</math>1.54</b>	78.68 $\pm$ 0.77
FFCL	20.78 $\pm$ 2.01	62.62 $\pm$ 1.04	78.48 $\pm$ 0.38	60.31 $\pm$ 2.92	63.20 $\pm$ 3.96	<b>8.50<math>\pm</math>1.24</b>	8.83 $\pm$ 0.28	62.93 $\pm$ 2.86	80.17 $\pm$ 1.89
ST-Transformer	10.83 $\pm$ 1.21	59.15 $\pm$ 1.95	79.66 $\pm$ 0.23	59.69 $\pm$ 3.58	58.40 $\pm$ 2.33	12.39 $\pm$ 0.46	10.69 $\pm$ 0.38	63.62 $\pm$ 3.01	76.95 $\pm$ 1.14
LaBraM	23.86 $\pm$ 2.09	70.75 $\pm$ 3.58	81.40 $\pm$ 0.19	60.26 $\pm$ 2.84	56.58 $\pm$ 3.22	16.10 $\pm$ 0.04	13.66 $\pm$ 1.46	56.43 $\pm$ 2.40	75.59 $\pm$ 2.60
CBraMod	25.69 $\pm$ 1.43	73.98 $\pm$ 2.84	78.91 $\pm$ 0.30	61.01 $\pm$ 4.57	60.09 $\pm$ 5.66	15.80 $\pm$ 0.14	15.71 $\pm$ 0.21	53.84 $\pm$ 4.40	75.29 $\pm$ 6.29
BrainHarmonix-F	7.71 $\pm$ 0.92	56.08 $\pm$ 0.76	77.94 $\pm$ 0.14	62.16 $\pm$ 1.15	62.78 $\pm$ 2.56	14.81 $\pm$ 0.49	<u>8.73<math>\pm</math>0.09</u>	63.11 $\pm$ 1.32	77.95 $\pm$ 2.36
Brain-OF Base	23.98 $\pm$ 0.29	73.99 $\pm$ 1.48	81.88 $\pm$ 0.17	68.23 $\pm$ 2.07	62.57 $\pm$ 1.19	12.09 $\pm$ 0.78	8.99 $\pm$ 0.14	58.95 $\pm$ 2.13	76.05 $\pm$ 0.44
Brain-OF Large	24.68 $\pm$ 0.37	<u>74.12<math>\pm</math>1.13</u>	<u>81.90<math>\pm</math>0.15</u>	<u>69.01<math>\pm</math>2.62</u>	<u>63.30<math>\pm</math>0.47</u>	11.71 $\pm$ 0.67	8.86 $\pm$ 0.21	62.85 $\pm$ 4.29	78.04 $\pm$ 1.59
Brain-OF Huge	<b>26.36<math>\pm</math>0.17</b>	<b>74.87<math>\pm</math>0.84</b>	<b>82.87<math>\pm</math>0.18</b>	<b>71.79<math>\pm</math>2.19</b>	<b>63.51<math>\pm</math>1.01</b>	9.51 $\pm$ 0.51	<b>7.87<math>\pm</math>0.22</b>	61.79 $\pm$ 1.29	<b>80.39<math>\pm</math>0.59</b>

Performance is reported as mean  $\pm$  standard deviation across five random seeds. The best result is highlighted in bold and the second-best result is underlined.

across fMRI, EEG and MEG modalities. In total, the pre-training dataset comprises **32,278 unique participants and 5,870,984 samples**. This diverse dataset integrates a wide range of M/EEG channel configurations and both 3T and 7T fMRI recordings from multiracial, multicultural international sites. Such heterogeneity in acquisition protocols, populations and modalities enables the construction of a general-purpose, omnifunctional brain foundation model. Further details on dataset descriptions and preprocessing are provided in Section A and Table 5.

**Downstream Tasks.** We evaluate Brain-OF on seven downstream tasks across 11 experiments spanning **fMRI, EEG and MEG** modalities in both unimodal and multimodal settings. To assess the generalizability of the model on EEG, we include emotion recognition (SEED-V), seizure detection (CHB-MIT) and abnormal detection (TUAB) as downstream tasks. For fMRI, two large multi-site datasets are used to evaluate diagnostic performance on neurodegenerative Alzheimer’s disease (ADNI) and neurodevelopmental attention deficit hyperactivity disorder (ADHD-200), respectively. In addition, brain age prediction (CamCAN) serves as a regression benchmark to evaluate unimodal MEG, unimodal fMRI, and multimodal MEG+fMRI fusion. A second multimodal dataset (LEMON) is further employed to assess age-group classification in unimodal EEG, unimodal fMRI, and multimodal EEG+fMRI settings. Together, these downstream tasks evaluate Brain-OF’s effectiveness on resting-state, task-state and ictal/interictal brain activity, while probing single-modality and cross-modality fusion scenarios. We adopt cross-subject/trial splits following (Wang et al., 2024a) for EEG datasets and a stratified split following (Kan et al., 2022) for fMRI datasets (7:1.5:1.5), ensuring strict subject-wise separation of training, validation and test sets. Detailed dataset configurations are provided in Table 1 and Section A.3.

## 4.2. Experiment Setups

**Pre-training Settings.** Brain-OF is released in three model variants: a 12-layer Brain-OF Base (47.5M parameters, 21.5M active parameters), a 24-layer Brain-OF Large (331M parameters, 150M active parameters) and a 36-layer Brain-OF Huge (1.7B parameters, 500M active parameters). All models are implemented using Python 3.11.11 and PyTorch 2.4.1+CUDA 12.1. Model training adopts the AdamW optimizer in BF16 precision with a global batch size of 7,168. The optimization follows a cosine-annealing schedule with a peak learning rate of  $3 \times 10^{-3}$ , weight decay of  $5 \times 10^{-2}$ , and optimizer states  $\beta = (0.9, 0.95)$  and  $\epsilon = 10^{-8}$ . Variable-length input signals are transformed and padded to a unified sequence length of 2,048. To stabilize routing, we employ an auxiliary-loss-free update for the router bias with coefficient  $\gamma = 10^{-3}$ . Pretraining is conducted on up to 56 compute nodes, each equipped with 4 NVIDIA A100 (40GB) GPUs (224 GPUs in total), for approximately six days. Comprehensive hyperparameter configurations are detailed in Section G.

**Baselines.** To provide a comprehensive comparison across modalities, we consider the following baseline models: task-specific models (ContraWR (Yang et al., 2023b), CNN-Transformer (Peh et al., 2022), FFCL (Li et al., 2022) and ST-Transformer (Song et al., 2021)), EEG foundation models (LaBraM (Jiang et al., 2024) and CBraMod (Wang et al., 2024a)), and the fMRI foundation model (BrainHarmonix-F (Dong et al., 2025)). Additional details on all baselines are provided in Section B.

**Evaluation Metrics.** We employ task-specific evaluation metrics for different downstream tasks. For binary classification tasks, we report Balanced Accuracy (BAC), which is also used as the primary metric for model checkpoint selection. In multi-class classification settings, Cohen’s Kappa is adopted as the primary evaluation metric. For regression tasks, performance is assessed using Mean Absolute Error

Table 3. Ablation studies on downstream tasks.

Methods	SEED-V	CHB-MIT	TUAB	ADNI	ADHD-200	CamCAN	CamCAN	LEMON	LEMON
	EEG	EEG	EEG	fMRI	fMRI	fMRI	MEG	fMRI	EEG
	Kappa(%) $\uparrow$	BAC(%) $\uparrow$	BAC(%) $\uparrow$	BAC(%) $\uparrow$	BAC(%) $\uparrow$	MAE $\downarrow$	MAE $\downarrow$	BAC(%) $\uparrow$	BAC(%) $\uparrow$
Brain-OF (Base)	<b>23.98</b> $\pm$ 0.29	<b>73.99</b> $\pm$ 1.48	<b>81.88</b> $\pm$ 0.17	<b>68.23</b> $\pm$ 2.07	<b>62.57</b> $\pm$ 1.19	<b>12.09</b> $\pm$ 0.78	<b>8.99</b> $\pm$ 0.14	<b>58.95</b> $\pm$ 2.13	<b>76.05</b> $\pm$ 0.44
<i>Objective Ablation</i>									
- w/o MTFM	21.52 $\pm$ 0.57	71.43 $\pm$ 2.30	81.49 $\pm$ 0.18	65.26 $\pm$ 1.83	<u>60.35</u> $\pm$ 1.50	12.80 $\pm$ 1.15	<b>8.96</b> $\pm$ 0.33	57.18 $\pm$ 1.91	<b>76.90</b> $\pm$ 0.51
<i>Modality Ablation</i>									
- w/o fMRI	<u>22.24</u> $\pm$ 0.27	<u>71.61</u> $\pm$ 0.90	80.98 $\pm$ 0.19	64.35 $\pm$ 1.77	59.94 $\pm$ 1.78	12.71 $\pm$ 0.51	9.16 $\pm$ 0.13	56.89 $\pm$ 3.68	<u>76.17</u> $\pm$ 0.54
- w/o EEG	19.35 $\pm$ 0.40	69.07 $\pm$ 1.42	81.86 $\pm$ 0.13	<u>67.37</u> $\pm$ 1.67	59.08 $\pm$ 1.15	12.30 $\pm$ 0.65	9.17 $\pm$ 0.27	<b>60.29</b> $\pm$ 2.82	75.61 $\pm$ 1.05
- w/o MEG	21.62 $\pm$ 0.35	70.93 $\pm$ 1.85	81.50 $\pm$ 0.19	<u>66.68</u> $\pm$ 2.43	60.13 $\pm$ 0.83	<u>12.25</u> $\pm$ 0.97	9.36 $\pm$ 0.15	56.68 $\pm$ 1.44	75.30 $\pm$ 1.03

(MAE). All reported results are presented as the mean and standard deviation over five random seeds. For each run, the best model is selected based on the primary metric on the validation set, and final performance is reported on a held-out test set.

### 4.3. Comparison with State-of-the-Art Baselines

Brain-OF is evaluated on a diverse set of downstream tasks including regression, binary and multi-class classification across EEG, fMRI, and MEG modalities. As detailed in Table 2, Brain-OF Huge achieves state-of-the-art performance, ranking first in 7 out of 9 tasks with an average rank of 1.8 across all evaluated settings. These results demonstrate its strong cross-modal generalization capability and robustness across heterogeneous neuroimaging modalities. We observe a consistent performance improvement as model capacity increases. Scaling from Brain-OF Base to Brain-OF Huge yields monotonic improvements across nearly all tasks. Notably, on the CamCAN (MEG) brain-age regression task, the MAE decreases from 8.99 (Base) to 7.87 (Huge), indicating that larger capacity effectively captures fine-grained, continuous biological variations. An important observation is that task-specific models (e.g., FFCL) occasionally outperform single-modality foundation models (e.g., LaBraM, BrainHarmonix-F) when tested on modalities different from their pretraining domain. This suggests that foundation models pretrained exclusively on a single modality may over-specialize in modality-specific signal characteristics, leading to negative transfer when applied to other modalities (e.g., EEG-pretrained models on fMRI or MEG tasks). In contrast, Brain-OF’s joint multimodal pretraining mitigates this issue by learning shared neural representations while still accommodating modality-specific differences.

### 4.4. Ablation Studies

To rigorously assess the contributions of the proposed MTFM pretraining objective and the role of heterogeneous modality integration, we conduct comprehensive ablation studies across multiple downstream tasks, as summarized in Table 3.

**Effectiveness of MTFM.** To isolate the benefit of dual-domain pretraining, we compare Brain-OF (pretrained with MTFM) against a baseline pretrained with a standard Masked Autoencoder objective. As shown in Table 3, replacing MTFM with conventional temporal masking consistently degrades performance across most tasks. This confirms that jointly reconstructing signals in both the time and frequency domains forces the model to capture richer neural dynamics than temporal reconstruction alone. The performance gains are particularly pronounced for tasks requiring complex neural signal decoding, such as SEED-V and CHB-MIT. In contrast, the improvements are relatively modest for more static demographic prediction tasks (e.g., CamCAN and LEMON), where fine-grained frequency dynamics may play a less dominant role.

**Cross-Modal Synergy and Modality Specificity.** We further examine the contribution of each modality by selectively removing fMRI, EEG, or MEG during pretraining. Interestingly, removing a specific modality does not always lead to a catastrophic performance drop on downstream tasks of that same modality. For instance, removing EEG data results in only a marginal drop on the TUAB (EEG) task. This suggests that Brain-OF learns robust modality-invariant representations, allowing knowledge transfer across modalities, while modality-specific data still provides additional benefits. In several cases, cross-modal data contributes more significantly than within-modality data. For example, on the ADHD-200 fMRI task, removing EEG data leads to a larger performance drop than removing fMRI data itself. Similarly, for the TUAB (EEG) dataset, the inclusion of fMRI data is critical for maximizing performance. This phenomenon may arise because cross-modal signals provide complementary, non-redundant information that serves as a strong inductive bias.

Overall, these ablation results demonstrate that Brain-OF benefits not only from joint heterogeneous modality but also from enforcing dual-domain reconstruction, validating the effectiveness of both the MTFM objective and the modality integration.

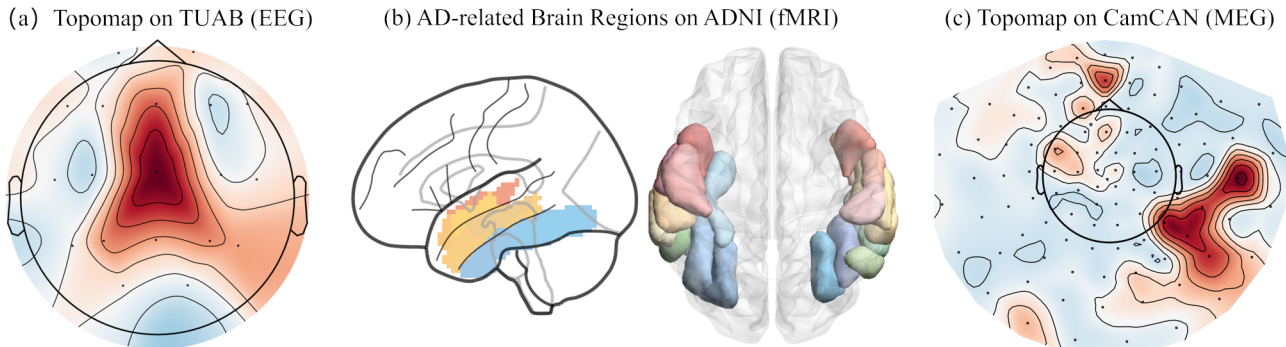


Figure 2. **Visualization of Brain-OF Interpretability.** (a) EEG channel contribution topomap for abnormality detection on TUAB. (b) top 10% most influential AD-related brain regions on ADNI. (c) MEG sensor contribution map for brain-age prediction on CamCAN.

#### 4.5. Performance Gains via Multimodal Fusion

Beyond unimodal evaluation, we assess multimodal fusion on two paired-modality benchmarks: brain-age prediction on CamCAN (fMRI + MEG) and age-group classification on LEMON (fMRI + EEG). Fusion is implemented via serial resampling with ARNESS, which integrates heterogeneous modalities into a unified fixed-length sequence without additional fusion modules or auxiliary alignment losses. Regarding sequence construction, we adopt an empirical ordering strategy in which the dominant modality (i.e., achieving higher unimodal performance) is placed at the end of the sequence to maximize its influence on the final representation. As shown in Table 4, multimodal fusion consistently outperforms unimodal baselines across nearly all model scales. For both tasks, electrophysiological signals (MEG/EEG) yield stronger unimodal performance than fMRI, reflecting the temporal sensitivity of these benchmarks. Importantly, incorporating fMRI further improves results by injecting complementary spatial information. For example, with Brain-OF Large, fusion reduces the CamCAN MAE to 8.78 (vs. 8.86 with MEG-only) and increases LEMON BAC to 78.32% (vs. 78.04% with EEG-only). These results demonstrate that Brain-OF effectively integrates complementary spatiotemporal information from disparate sources to achieve superior predictive power.

#### 4.6. Visualization of Model Explanations

To interpret the representations learned by Brain-OF Base, we employ the occlusion method (Zeiler & Fergus, 2014) to quantify the contribution of each channel/ROI to the model’s predictive performance across three representative downstream tasks. As shown in Figure 2(a), the topomap of EEG channel contribution for abnormality detection on TUAB strongly focuses on central and frontal scalp regions, indicating that Brain-OF captures spatially discriminative EEG biomarkers associated with abnormal neural activity. For Alzheimer’s disease (AD) classification on ADNI (Figure 2(b)), the top 10% most influential ROIs are primarily located in the fusiform gyrus, as well as the middle and

Table 4. **Performance benefits of multimodal fusion.** Comparison between unimodal baselines (fMRI-only and MEG/EEG-only) and multimodal fusion on CamCAN (fMRI + MEG) and LEMON (fMRI + EEG), demonstrating Brain-OF’s ability to effectively integrate complementary cross-modal information.

Model	Modality	CamCAN MAE ↓	LEMON BAC(%) ↑
Base	fMRI-only	12.09 ± 0.78	58.95 ± 2.13
	MEG/EEG-only	8.99 ± 0.14	76.05 ± 0.44
	<b>Multimodal Fusion</b>	<b>8.87 ± 0.09</b>	<b>76.77 ± 0.60</b>
Large	fMRI-only	11.71 ± 0.67	62.85 ± 4.29
	MEG/EEG-only	8.86 ± 0.21	78.04 ± 1.59
	<b>Multimodal Fusion</b>	<b>8.78 ± 0.07</b>	<b>78.32 ± 1.64</b>
Huge	fMRI-only	9.51 ± 0.51	61.79 ± 1.29
	MEG/EEG-only	7.87 ± 0.22	80.39 ± 0.59
	<b>Multimodal Fusion</b>	<b>8.21 ± 0.11</b>	<b>81.10 ± 0.54</b>

inferior temporal gyri. These regions are well known to be affected by cortical atrophy in AD (Convit et al., 2000), suggesting that Brain-OF relies on neurobiologically meaningful features rather than spurious correlations. Finally, the MEG sensor-level contribution map for brain-age prediction on CamCAN (Figure 2(c)) reveals distinct clusters of highly informative sensors, particularly over temporal-parietal regions. Taken together, these visualizations indicate that Brain-OF learns interpretable and biologically plausible representations across modalities, validating its suitability for neuroscientific analysis and clinical applications.

## 5. Conclusion

In this work, we introduce **Brain-OF**, the first omnifunctional brain foundation model designed to harness the complementary spatiotemporal characteristics of fMRI, EEG and MEG. To address the heterogeneity of signal resolutions across modalities, we propose the *Any-Resolution Neural Signal Sampler*, which projects diverse inputs into a shared semantic space. Our architecture further addresses semantic complexity through a backbone integrating *DINT attention* and *Sparse Mixture of Experts*, where shared and routed experts capture modality-invariant knowledge and

modality-specific representations, respectively. Crucially, to enforce deep understanding of brain dynamics, we propose *Masked Temporal-Frequency Modeling*, a pretraining objective that compels joint reconstruction of signals in both time and frequency domains. Extensive experiments across unimodal and multimodal tasks demonstrate that Brain-OF achieves superior performance, highlighting the benefits of large-scale joint pretraining across heterogeneous brain signals. We hope that Brain-OF paves the way toward general-purpose, scalable and interpretable brain foundation models for both unimodal and cross-modal neuroscience applications.

## Impact Statement

This work presents Brain-OF, an omnifunctional foundation model jointly pretrained on fMRI, EEG and MEG, representing a significant advance toward unifying heterogeneous neuroimaging modalities within a single framework. Compared to single-modality foundation models, Brain-OF exhibits potentially stronger generalization capabilities, even to unseen or specialized functional modalities. Consequently, Brain-OF has a broader impact on multimodal fusion in neuroscience research and clinical applications, empowering researchers to integrate the high spatial resolution of fMRI with the temporal precision of EEG/MEG for more accurate diagnosis in epilepsy, neurodegenerative diseases and cognitive disorders. Moreover, by transferring knowledge from capital-intensive modalities (fMRI/MEG) to accessible, wearable ones (EEG), this work accelerates the deployment of high-performance neurotechnologies in real-world and portable settings. We release Brain-OF Huge, one of the largest open-source brain foundation models to date. This provides a reliable, pre-validated backbone for the neuroscience and brain-computer interface community, substantially lowering the barrier to entry for researchers who lack resources to pretrain large-scale models from scratch. By enabling the reuse of rich, cross-modal representations, we aim to broaden access to powerful neural representations and foster a collaborative, data-centric ecosystem for future neuroimaging research.

## References

- ADHD-200-consortium. The adhd-200 consortium: a model to advance the translational potential of neuroimaging in clinical neuroscience. *Frontiers in systems neuroscience*, 6:62, 2012.
- Alayrac, J.-B., Donahue, J., Luc, P., Miech, A., Barr, I., Hasson, Y., Lenc, K., Mensch, A., Millican, K., Reynolds, M., et al. Flamingo: a visual language model for few-shot learning. *Advances in neural information processing systems*, 35:23716–23736, 2022.
- Babayan, A., Erbey, M., Kumral, D., Reinelt, J. D., Reiter, A. M., Röbbig, J., Schaare, H. L., Uhlig, M., Anwender, A., Bazin, P.-L., et al. A mind-brain-body dataset of mri, eeg, cognition, emotion, and peripheral physiology in young and old adults. *Scientific data*, 6(1):1–21, 2019.
- Blokland, G. A., McMahon, K. L., Thompson, P. M., Martin, N. G., de Zubicaray, G. I., and Wright, M. J. Heritability of working memory brain activation. *Journal of Neuroscience*, 31(30):10882–10890, 2011.
- Botvinik-Nezer, R., Petre, B., Ceko, M., Lindquist, M. A., Friedman, N. P., and Wager, T. D. Placebo treatment affects brain systems related to affective and cognitive processes, but not nociceptive pain. *Nature communications*, 15(1):6017, 2024.
- Cang, Y., Liu, Y., Zhang, X., Zhao, E., and Shi, L. Dint transformer. *arXiv preprint arXiv:2501.17486*, 2025.
- Caro, J. O., Fonseca, A. H. d. O., Averill, C., Rizvi, S. A., Rosati, M., Cross, J. L., Mittal, P., Zappala, E., Levine, D., Dhodapkar, R. M., et al. Brainlm: A foundation model for brain activity recordings. *bioRxiv*, pp. 2023–09, 2023.
- Chau, G., Wang, C., Talukder, S., Subramaniam, V., Soedar-madji, S., Yue, Y., Katz, B., and Barbu, A. Population transformer: Learning population-level representations of neural activity. *ArXiv*, pp. arXiv–2406, 2025.
- Chen, J., Wang, X., Huang, C., Hu, X., Shen, X., and Zhang, D. A large finer-grained affective computing eeg dataset. *Scientific Data*, 10(1):740, 2023.
- Chen, X., Lu, B., Li, H.-X., Li, X.-Y., Wang, Y.-W., Castellanos, F. X., Cao, L.-P., Chen, N.-X., Chen, W., Cheng, Y.-Q., et al. The direct consortium and the rest-meta-mdd project: towards neuroimaging biomarkers of major depressive disorder. *Psychoradiology*, 2(1):32–42, 2022.
- Chowdhury, N. S., Bi, C., Furman, A. J., Chiang, A. K., Skippen, P., Si, E., Millard, S. K., Margerison, S. M., Spies, D., Keaser, M. L., Silva, J. T. D., Chen, S., Schabrun, S. M., and Seminowicz, D. A. "predict". 2025a. doi: doi:10.18112/openneuro.ds005486.v1.0.1.
- Chowdhury, N. S., Bi, C., Furman, A. J., Chiang, A. K., Skippen, P., Si, E., Millard, S. K., Margerison, S. M., Spies, D., Keaser, M. L., et al. Predicting individual pain sensitivity using a novel cortical biomarker signature. *JAMA neurology*, 82(3):237–246, 2025b.
- Convit, A., De Asis, J., De Leon, M., Tarshish, C., De Santi, S., and Rusinek, H. Atrophy of the medial occipitotemporal, inferior, and middle temporal gyri in non-demented elderly predict decline to alzheimer’s disease. *Neurobiology of aging*, 21(1):19–26, 2000.

- Di Martino, A., Yan, C.-G., Li, Q., Denio, E., Castellanos, F. X., Alaerts, K., Anderson, J. S., Assaf, M., Bookheimer, S. Y., Dapretto, M., et al. The autism brain imaging data exchange: towards a large-scale evaluation of the intrinsic brain architecture in autism. *Molecular psychiatry*, 19(6): 659–667, 2014.
- Di Martino, A., O’connor, D., Chen, B., Alaerts, K., Anderson, J. S., Assaf, M., Balsters, J. H., Baxter, L., Beggiano, A., Bernaerts, S., et al. Enhancing studies of the connectome in autism using the autism brain imaging data exchange ii. *Scientific data*, 4(1):1–15, 2017.
- Dong, Z., Li, R., Wu, Y., Nguyen, T. T., Chong, J., Ji, F., Tong, N., Chen, C., and Zhou, J. H. Brain-jepa: Brain dynamics foundation model with gradient positioning and spatiotemporal masking. *Advances in Neural Information Processing Systems*, 37:86048–86073, 2024.
- Dong, Z., Li, R., Chong, J. S. X., Dehestani, N., Teng, Y., Lin, Y., Li, Z., Zhang, Y., Xie, Y., Ooi, L. Q. R., et al. Brain harmony: A multimodal foundation model unifying morphology and function into 1d tokens. *arXiv preprint arXiv:2509.24693*, 2025.
- Esteban, O., Markiewicz, C. J., Blair, R. W., Moodie, C. A., Isik, A. I., Erramuzpe, A., Kent, J. D., Goncalves, M., DuPre, E., Snyder, M., et al. fmriprep: a robust preprocessing pipeline for functional mri. *Nature methods*, 16(1):111–116, 2019.
- Fan, L., Li, H., Zhuo, J., Zhang, Y., Wang, J., Chen, L., Yang, Z., Chu, C., Xie, S., Laird, A. R., et al. The human brainnetome atlas: a new brain atlas based on connectonal architecture. *Cerebral cortex*, 26(8):3508–3526, 2016.
- Ge, J., Yang, G., Han, M., Zhou, S., Men, W., Qin, L., Lyu, B., Li, H., Wang, H., Rao, H., et al. Increasing diversity in connectomics with the chinese human connectome project. *Nature Neuroscience*, 26(1):163–172, 2023.
- Getzmann, S., Gajewski, P. D., Schneider, D., and Wascher, E. Resting-state eeg data before and after cognitive activity across the adult lifespan and a 5-year follow-up. *Scientific Data*, 11(1):988, 2024.
- Goldberger, A. L., Amaral, L. A., Glass, L., Hausdorff, J. M., Ivanov, P. C., Mark, R. G., Mietus, J. E., Moody, G. B., Peng, C.-K., and Stanley, H. E. Physiobank, physiotoolkit, and physionet: components of a new research resource for complex physiologic signals. *circulation*, 101(23): e215–e220, 2000.
- Gramfort, A., Luessi, M., Larson, E., Engemann, D. A., Strohmeier, D., Brodbeck, C., Parkkonen, L., and Hämäläinen, M. S. Mne software for processing meg and eeg data. *neuroimage*, 86:446–460, 2014.
- Guo, H., Abdellatif, F., Fu, Y., Shah, N. J., Morrison, A., and Dammers, J. Xaiguiformer: explainable artificial intelligence guided transformer for brain disorder identification. In *The Thirteenth International Conference on Learning Representations*, 2025.
- Han, X., Zhang, Z., Ding, N., Gu, Y., Liu, X., Huo, Y., Qiu, J., Yao, Y., Zhang, A., Zhang, L., et al. Pre-trained models: Past, present and future. *Ai Open*, 2:225–250, 2021.
- He, B., Sohrabpour, A., Brown, E., and Liu, Z. Electrophysiological source imaging: a noninvasive window to brain dynamics. *Annual review of biomedical engineering*, 20(1):171–196, 2018.
- Jack Jr, C. R., Bernstein, M. A., Fox, N. C., Thompson, P., Alexander, G., Harvey, D., Borowski, B., Britson, P. J., L. Whitwell, J., Ward, C., et al. The alzheimer’s disease neuroimaging initiative (adni): Mri methods. *Journal of Magnetic Resonance Imaging: An Official Journal of the International Society for Magnetic Resonance in Medicine*, 27(4):685–691, 2008.
- Jansen, M., Zwiers, M., Marques, J., Chan, K., Amelink, J. J., Altgassen, M., Oosterman, J., and Norris, D. The Advanced BBrain Imaging database on ageing and Memory (ABRIM) study: MRI collection, 2023. URL <https://doi.org/10.34973/7q0a-vj19>.
- Jiang, W.-B., Zhao, L.-M., and Lu, B.-L. Large brain model for learning generic representations with tremendous eeg data in bci. *arXiv preprint arXiv:2405.18765*, 2024.
- Jiang, W.-B., Fu, X., Ding, Y., and Guan, C. Towards robust multimodal physiological foundation models: Handling arbitrary missing modalities. *arXiv preprint arXiv:2504.19596*, 2025a.
- Jiang, W.-B., Liu, X.-H., Zheng, W.-L., and Lu, B.-L. Seed-vii: A multimodal dataset of six basic emotions with continuous labels for emotion recognition. *IEEE Transactions on Affective Computing*, 16(2):969–985, 2025b. doi: 10.1109/TAFFC.2024.3485057.
- Jung, H., Amini, M., Hunt, B. J., Murphy, E. I., Sadil, P., Halchenko, Y. O., Petre, B., Miao, Z., Kragel, P. A., Han, X., et al. Spacetop: A multimodal fmri dataset unifying naturalistic processes with a rich array of experimental tasks. *Scientific Data*, 12(1):1465, 2025.
- Kan, X., Dai, W., Cui, H., Zhang, Z., Guo, Y., and Yang, C. Brain network transformer. *Advances in Neural Information Processing Systems*, 35:25586–25599, 2022.
- Kaplan, J., McCandlish, S., Henighan, T., Brown, T. B., Chess, B., Child, R., Gray, S., Radford, A., Wu, J., and Amodei, D. Scaling laws for neural language models. *arXiv preprint arXiv:2001.08361*, 2020.

- Kostas, D., Aroca-Ouellette, S., and Rudzicz, F. Bendr: Using transformers and a contrastive self-supervised learning task to learn from massive amounts of eeg data. *Frontiers in Human Neuroscience*, 15:653659, 2021.
- Li, H., Ding, M., Zhang, R., and Xiu, C. Motor imagery eeg classification algorithm based on cnn-lstm feature fusion network. *Biomedical signal processing and control*, 72: 103342, 2022.
- Li, Z., Tao, L.-Y., Ma, R.-X., Zheng, W.-L., and Lu, B.-L. Investigating the effects of sleep conditions on emotion responses with eeg signals and eye movements. *IEEE Transactions on Affective Computing*, 2025. doi: 10.1109/TAFFC.2025.3572504.
- Liu, W., Qiu, J.-L., Zheng, W.-L., and Lu, B.-L. Comparing recognition performance and robustness of multimodal deep learning models for multimodal emotion recognition. *IEEE Transactions on Cognitive and Developmental Systems*, 2021.
- Liu, X.-H., Liu, Y.-K., Wang, Y., Ren, K., Shi, H., Wang, Z., Li, D., Lu, B.-L., and Zheng, W.-L. EEG2Video: Towards decoding dynamic visual perception from EEG signals. *Advances in Neural Information Processing Systems (NeurIPS)*, 2024.
- Logothetis, N. K. and Pfeuffer, J. On the nature of the bold fmri contrast mechanism. *Magnetic resonance imaging*, 22(10):1517–1531, 2004.
- Luo, Y., Liu, W., Li, H., Lu, Y., and Lu, B.-L. A cross-scenario and cross-subject domain adaptation method for driving fatigue detection. *Journal of Neural Engineering*, 21(4):046004, jul 2024. doi: 10.1088/1741-2552/ad546d. URL <https://dx.doi.org/10.1088/1741-2552/ad546d>.
- Maaten, L. v. d. and Hinton, G. Visualizing data using t-sne. *Journal of machine learning research*, 9(Nov): 2579–2605, 2008.
- McNabb, C. B., Driver, I. D., Hyde, V., Hughes, G., Chandler, H. L., Thomas, H., Allen, C., Messaritaki, E., Hodgetts, C. J., Hedge, C., et al. Wand: A multi-modal dataset integrating advanced mri, meg, and tms for multi-scale brain analysis. *Scientific Data*, 12(1):220, 2025.
- Nastase, S. A., Liu, Y.-F., Hillman, H., Zadbood, A., Hasenfratz, L., Keshavarzian, N., Chen, J., Honey, C. J., Yeshurun, Y., Regev, M., et al. The “narratives” fmri dataset for evaluating models of naturalistic language comprehension. *Scientific data*, 8(1):250, 2021.
- Niso, G., Rogers, C., Moreau, J. T., Chen, L.-Y., Madjar, C., Das, S., Bock, E., Tadel, F., Evans, A. C., Jolicoeur, P., et al. Omega: the open meg archive. *Neuroimage*, 124: 1182–1187, 2016.
- Obeid, I. and Picone, J. The temple university hospital eeg data corpus. *Frontiers in neuroscience*, 10:196, 2016.
- Park, D. C., Hennessee, J. P., Smith, E. T., Chan, M. Y., Chen, X., Dakanali, M., Farrell, M. E., Liu, P., Lu, H., Rofsky, N., et al. The dallas lifespan brain study: A comprehensive adult lifespan data set of brain and cognitive aging. *Scientific Data*, 12(1):846, 2025.
- Peh, W. Y., Yao, Y., and Dauwels, J. Transformer convolutional neural networks for automated artifact detection in scalp eeg. In *2022 44th Annual International Conference of the IEEE Engineering in Medicine & Biology Society (EMBC)*, pp. 3599–3602. IEEE, 2022.
- Poldrack, R. A., Congdon, E., Triplett, W., Gorgolewski, K., Karlsgodt, K., Mumford, J., Sabb, F., Freimer, N., London, E., Cannon, T., et al. A phenome-wide examination of neural and cognitive function. *Scientific data*, 3(1): 1–12, 2016.
- Radford, A., Narasimhan, K., Salimans, T., Sutskever, I., et al. Improving language understanding by generative pre-training. 2018.
- Schalk, G., McFarland, D. J., Hinterberger, T., Birbaumer, N., and Wolpaw, J. R. Bci2000: a general-purpose brain-computer interface (bci) system. *IEEE Transactions on biomedical engineering*, 51(6):1034–1043, 2004.
- Schoffelen, J.-M., Oostenveld, R., Lam, N. H., Uddén, J., Hultén, A., and Hagoort, P. A 204-subject multimodal neuroimaging dataset to study language processing. *Scientific data*, 6(1):17, 2019.
- Shoeb, A. H. *Application of machine learning to epileptic seizure onset detection and treatment*. PhD thesis, Massachusetts Institute of Technology, 2009.
- Sinclair, B., Hansell, N. K., Blokland, G. A., Martin, N. G., Thompson, P. M., Breakspear, M., de Zubicaray, G. I., Wright, M. J., and McMahon, K. L. Heritability of the network architecture of intrinsic brain functional connectivity. *Neuroimage*, 121:243–252, 2015.
- Snoek, L., van der Miesen, M. M., Beemsterboer, T., Van Der Leij, A., Eigenhuis, A., and Steven Scholte, H. The amsterdam open mri collection, a set of multimodal mri datasets for individual difference analyses. *Scientific data*, 8(1):85, 2021.
- Song, Y., Jia, X., Yang, L., and Xie, L. Transformer-based spatial-temporal feature learning for eeg decoding. *arXiv preprint arXiv:2106.11170*, 2021.
- Spreng, R. N., Setton, R., Alter, U., Cassidy, B. N., Darboh, B., DuPre, E., Kantarovich, K., Lockrow, A. W.,

- Mwilambwe-Tshilobo, L., Luh, W.-M., et al. Neurocognitive aging data release with behavioral, structural and multi-echo functional mri measures. *Scientific Data*, 9(1):119, 2022.
- Su, J., Ahmed, M., Lu, Y., Pan, S., Bo, W., and Liu, Y. Roformer: Enhanced transformer with rotary position embedding. *Neurocomputing*, 568:127063, 2024.
- Taylor, J. R., Williams, N., Cusack, R., Auer, T., Shafto, M. A., Dixon, M., Tyler, L. K., Henson, R. N., et al. The cambridge centre for ageing and neuroscience (camcan) data repository: Structural and functional mri, meg, and cognitive data from a cross-sectional adult lifespan sample. *neuroimage*, 144:262–269, 2017.
- Tobe, R. H., MacKay-Brandt, A., Lim, R., Kramer, M., Breland, M. M., Tu, L., Tian, Y., Trautman, K. D., Hu, C., Sangoi, R., et al. A longitudinal resource for studying connectome development and its psychiatric associations during childhood. *Scientific data*, 9(1):300, 2022.
- Van Dijk, H., Van Wingen, G., Denys, D., Olbrich, S., Van Ruth, R., and Arns, M. The two decades brainclinics research archive for insights in neurophysiology (tdbrain) database. *Scientific data*, 9(1):333, 2022.
- Van Essen, D. C., Smith, S. M., Barch, D. M., Behrens, T. E., Yacoub, E., Ugurbil, K., Consortium, W.-M. H., et al. The wu-minn human connectome project: an overview. *Neuroimage*, 80:62–79, 2013.
- Wang, C., Subramaniam, V., Yaari, A. U., Kreiman, G., Katz, B., Cases, I., and Barbu, A. Brainbert: Self-supervised representation learning for intracranial recordings. *arXiv preprint arXiv:2302.14367*, 2023.
- Wang, J., Zhao, S., Luo, Z., Zhou, Y., Jiang, H., Li, S., Li, T., and Pan, G. Cbramod: A criss-cross brain foundation model for eeg decoding. *arXiv preprint arXiv:2412.07236*, 2024a.
- Wang, L., Gao, H., Zhao, C., Sun, X., and Dai, D. Auxiliary-loss-free load balancing strategy for mixture-of-experts. *arXiv preprint arXiv:2408.15664*, 2024b.
- Wei, D., Zhuang, K., Ai, L., Chen, Q., Yang, W., Liu, W., Wang, K., Sun, J., and Qiu, J. Structural and functional brain scans from the cross-sectional southwest university adult lifespan dataset. *Scientific data*, 5(1):1–10, 2018.
- Wheless, J. W., Castillo, E., Maggio, V., Kim, H. L., Breier, J. I., Simos, P. G., and Papanicolaou, A. C. Magnetoencephalography (meg) and magnetic source imaging (msi). *The neurologist*, 10(3):138–153, 2004.
- Xiao, Q., Cui, Z., Zhang, C., Chen, S., Wu, W., Thwaites, A., Woolgar, A., Zhou, B., and Zhang, C. Brainomni: A brain foundation model for unified eeg and meg signals. *arXiv preprint arXiv:2505.18185*, 2025.
- Yang, B., Rong, F., Xie, Y., Li, D., Zhang, J., Li, F., Shi, G., and Gao, X. A multi-day and high-quality eeg dataset for motor imagery brain-computer interface. *Scientific Data*, 12(1):488, 2025.
- Yang, C., Westover, M., and Sun, J. Biot: Biosignal transformer for cross-data learning in the wild. *Advances in Neural Information Processing Systems*, 36:78240–78260, 2023a.
- Yang, C., Xiao, C., Westover, M. B., and Sun, J. Self-supervised electroencephalogram representation learning for automatic sleep staging: model development and evaluation study. *JMIR AI*, 2(1):e46769, 2023b.
- Yang, Y., Ye, C., Su, G., Zhang, Z., Chang, Z., Chen, H., Chan, P., Yu, Y., and Ma, T. Brainmass: Advancing brain network analysis for diagnosis with large-scale self-supervised learning. *IEEE transactions on medical imaging*, 43(11):4004–4016, 2024.
- Ye, T., Dong, L., Xia, Y., Sun, Y., Zhu, Y., Huang, G., and Wei, F. Differential transformer. *arXiv preprint arXiv:2410.05258*, 2024.
- Yi, K., Wang, Y., Ren, K., and Li, D. Learning topology-agnostic eeg representations with geometry-aware modeling. *Advances in Neural Information Processing Systems*, 36:53875–53891, 2023.
- Zeiler, M. D. and Fergus, R. Visualizing and understanding convolutional networks. In *European conference on computer vision*, pp. 818–833. Springer, 2014.
- Zheng, W.-L. and Lu, B.-L. Investigating critical frequency bands and channels for EEG-based emotion recognition with deep neural networks. *IEEE Transactions on Autonomous Mental Development*, 7(3):162–175, 2015. doi: 10.1109/TAMD.2015.2431497.
- Zheng, W.-L. and Lu, B.-L. A multimodal approach to estimating vigilance using eeg and forehead eeg. *Journal of Neural Engineering*, 14(2):026017, 2017. URL <http://stacks.iop.org/1741-2552/14/i=2/a=026017>.
- Zhou, Y., Wu, J., Ren, Z., Yao, Z., Lu, W., Peng, K., Zheng, Q., Song, C., Ouyang, W., and Gou, C. Csbrain: A cross-scale spatiotemporal brain foundation model for eeg decoding. *arXiv preprint arXiv:2506.23075*, 2025.
- Zuo, X.-N., Anderson, J. S., Bellec, P., Birn, R. M., Biswal, B. B., Blautzik, J., Breitner, J., Buckner, R. L., Calhoun, V. D., Castellanos, F. X., et al. An open science resource for establishing reliability and reproducibility in functional connectomics. *Scientific data*, 1(1):1–13, 2014.

## A. Details of Datasets

In this study, we integrate three heterogeneous functional brain imaging modalities (i.e., fMRI, EEG and MEG) to develop the omnifunctional brain foundation model (Brain-OF). These modalities differ substantially in their temporal, spatial, and spectral resolutions, giving rise to both semantic richness and considerable heterogeneity. Within each modality, further variability arises from heterogeneous acquisition protocols and scanners across international sites, reflected in diverse sampling rates (MEG/EEG), repetition times and field strengths (3 T vs. 7 T for fMRI), number of channels/sensors, recording durations and experimental paradigms (resting vs. task state).

Table 5. Summary of all pretraining datasets, covering 3 heterogeneous functional neuroimaging modalities (fMRI, EEG, MEG) across 37 public datasets, encompassing over 32K unique participants, approximately 5.9M samples, and 2.8 TB of preprocessed data.

Modalities	Datasets	Paradigms	SR / TR	# Channels / ROIs	Durations	# Participants	# Samples
EEG	FACED	task	250Hz	32	10s	123	10,332
	PhysioNet-MI	task	160Hz	64	4s	109	18,697
	PREDICT	rest	5,000Hz	63	10s	159	17,511
	REEG-BACA	rest	1,000Hz	64	10s	608	53,089
	SEED	task	1,000Hz	62	10s	15	14,895
	SEED-DV	task	1,000Hz	62	10s	20	7,644
	SEED-SD	task	1,000Hz	62	10s	40	38,120
	SEED-VIG	task	200Hz	17	8s	21	20,332
	SEED-VII	task	1,000Hz	62	10s	20	26,257
	SEED-VLA/VRW	task	300Hz	18	10s	20	17,287
	TDBRAIN	rest	500Hz	26	10s	1,274	26,422
	TUEG	rest	250Hz	19	10s	13,928	4,562,151
WBCIC-MI	task	1,000Hz	58	4s	62	40,290	
fMRI	ABIDE-I	rest	multi-site	246	-	1,112	1,152
	ABIDE-II	rest	multi-site	246	-	1,114	1,614
	ABRIM	rest & task	1,000ms	246	320s	282	562
	AOMIC-ID1000	task	2,200ms	246	660s	881	881
	AOMIC-PIOP1	rest & task	750ms	246	360s	216	1,236
	AOMIC-PIOP2	rest & task	2,000ms	246	480s	226	896
	CHCP	rest & task	710ms	246	227s	366	3,379
	CoRR	rest	multi-site	246	-	1,629	5,212
	DLBS	rest & task	2,000ms	246	374s	464	6,839
	NADR	rest	3,000ms	246	606s	301	596
	Narratives	task	1,500ms	246	480s	345	1,321
	NKI-RS	rest	1,400ms	246	448s	1,344	16,408
	Paingnet placebo	task	460ms	246	132s	395	3,143
	QTIM	rest & task	2,100ms	246	315s	1,202	2,453
	REST-meta-MDD	rest	multi-site	116	-	2,380	2,380
	SALD	rest	2,000ms	246	480s	493	493
	SpaceTop	task	460ms	246	200s	101	11,660
UCLA CNP	rest & task	2,000ms	246	304s	272	1,969	
MEG / Multimodal	CamCAN-MEG	rest & task	1,000Hz	306	2s	456	279,965
	CamCAN-fMRI	rest & task	1,970ms	246	520s	465	1,763
	HCP-YA-MEG	rest & task	2,000Hz	248	2s	89	241,115
	HCP-YA-fMRI	rest & task	720ms	246	230s	1,113	32,281
	LEMON-EEG	rest	2,500Hz	61	10s	144	12,235
	LEMON-fMRI	rest	1,400ms	246	448s	160	320
	MOUS-MEG	rest & task	1,200Hz	275	2s	204	66,322
	MOUS-fMRI	rest & task	1,680ms	246	420s	204	678
	OMEGA	rest	2,400Hz	275	2s	644	164,834
	WAND-MEG	rest & task	1,200Hz	275	2s	170	155,474
WAND-fMRI	rest & task	2,000ms	246	638s	170	776	
<b>Total</b>	<b>fMRI, EEG, MEG</b>	<b>rest &amp; task</b>	<b>-</b>	<b>-</b>	<b>-</b>	<b>32,278</b>	<b>5,870,984</b>

Some datasets include multiple sampling rates (SR) or repetition times (TR) due to differences in acquisition protocols across different phases or paradigms (e.g., resting-state vs. task-based scans). For conciseness, we report the primary SR/TR for each dataset in the ‘‘SR / TR’’ column. Similarly, the reported durations primarily correspond to resting-state recordings. For detailed information, please refer to the original publications. ROIs: regions of interest.

This diversity further supports the construction of a pluralistic pretraining corpus spanning multiracial, multicultural

populations, including both healthy individuals and clinical patients. In total, our pretraining dataset aggregates 37 publicly available datasets across fMRI, EEG and MEG, comprising 32,278 unique participants, 5,870,984 samples, and 2.8 TB of preprocessed data. Detailed statistics for each dataset can be found in Table 5.

### A.1. Data Preprocessing

If the public datasets provide official preprocessed data, we use them directly. Otherwise, we apply minimal, modality-specific preprocessing pipelines to remove artifacts. Raw EEG and MEG signals are preprocessed using MNE-Python (Gramfort et al., 2014), and fMRI data are preprocessed with fMRIPrep (Esteban et al., 2019). After preprocessing, z-score normalization is applied to all signals to harmonize their value ranges across fMRI, EEG and MEG.

**EEG.** To enhance stationarity, the initial and final 10 seconds of EEG signals are discarded. Signals are then band-pass filtered (1–80 Hz, zero-phase Hamming-windowed sinc FIR, –6 dB cutoff) and notched at the local power-line frequency (50 or 60 Hz). Filtered signals are resampled to 200 Hz, segmented into non-overlapping 10-second samples for resting-state data, and re-referenced to the common average.

**MEG.** MEG preprocessing similarly undergoes band-pass filtering (1–80 Hz, zero-phase Hamming-windowed sinc FIR, –6 dB cutoff) and notching at the power-line frequency. Filtered signals are resampled to 200 Hz and segmented into non-overlapping 2-second samples for resting-state recordings.

**fMRI.** For each BOLD series, a reference volume and its skull-stripped version are estimated. Head-motion parameters (volume-to-reference transforms and corresponding rotations/translations) are computed, followed by slice-timing correction using 3dTshift (AFNI). Functional volumes are co-registered to the T1-weighted anatomical reference via boundary-based registration (9 degrees of freedom) to minimize distortions. Motion correction, susceptibility distortion correction, BOLD-to-T1w, and T1w-to-template (MNI152NLin2009cAsym) warps are concatenated and applied in one interpolation step using antsApplyTransforms (ANTs). Nuisance regressors, including global signal, mean signals from white matter and CSF, tCompCor, aCompCor, framewise displacement, six motion parameters, DVARS, and spike regressors, are regressed out. Residual signals are spatially smoothed (6 mm FWHM Gaussian kernel) and subjected to Wishart filtering. Finally, regional time series are extracted from 246 parcels using the Brainnetome atlas (Fan et al., 2016).

### A.2. Pretraining Datasets

- **FACED** (Chen et al., 2023) is a large finer-grained affective computing EEG dataset comprising 32-channel recordings at sampling rate of 250 or 1,000 Hz from 123 subjects (ages 17-38). Each participant was instructed to watch 28 emotion-elicitation video clips spanning nine discrete emotional states: amusement, inspiration, joy, tenderness, anger, fear, disgust, sadness and neutral emotion.
- **PhysioNet-MI** (Schalk et al., 2004) is a large-scale motor imagery EEG collections, comprising 64-channel recordings (160 Hz sampling rate) from 109 healthy participants performing left fist, right fist, both fists, and both feet imagery. For pretraining, we use 4-second trials after preprocessing.
- **PREDICT** (Chowdhury et al., 2025a;b) is a longitudinal pain-related EEG dataset comprising 5-minute, eyes-closed, 63-channel resting-state recordings from 159 participants (ages 18–44) with no history of chronic pain, neurological disorders, or psychiatric conditions. EEG data were collected on Days 0, 2, and 5 of the experimental protocol, providing multiple sessions per participant for identifying individual pain sensitivity in healthy adults.
- **REEG-BACA** (Getzmann et al., 2024) is a large-scale longitudinal resting-state EEG dataset collected from 608 participants (ages 20-70), with 208 participants returning for a follow-up session approximately 5 years later. High-density rs-EEG was acquired using a 64-channel elastic cap (10–20 system) at 1,000 Hz sampling rate. Recordings were obtained both before and after a 2-hour battery of cognitive tasks.
- **SEED Series** is a family of EEG datasets designed for affective computing and related cognitive neuroscience research. It includes **SEED** (Zheng & Lu, 2015), **SEED-VIG** (Zheng & Lu, 2017), **SEED-VII** (Jiang et al., 2025b), **SEED-VLA/VRW** (Luo et al., 2024), **SEED-DV** (Liu et al., 2024) and **SEED-SD** (Li et al., 2025). All datasets were recorded using a 62-channel ESI NeuroScan system at a 1,000 Hz sampling rate during emotion-related paradigms spanning positive, negative and neutral valence, as well as more fine-grained affective states (e.g., amusement, fear, sadness). In total, the SEED Series provides EEG recordings from 136 unique participants, predominantly young adults.

- **TDBRAIN** (Van Dijk et al., 2022) is a large single-site lifespan EEG database (ages 5–89), comprising resting-state recordings from 1,274 psychiatric patients. The psychophysiological data include 26 channel EEG acquired at a sampling rate of 500 Hz.
- **TUEG** (Obeid & Picone, 2016) is the largest publicly available collection of clinical EEG dataset, comprising 69,652 recordings from 14,987 subjects across 26,846 sessions collected at Temple University Hospital. The dataset exhibits substantial variability in channel configurations, sampling rates and recording durations, reflecting the heterogeneity of real-world clinical practice. To prevent information leakage and ensure reliable downstream evaluation, we exclude all subjects that appear in the TUAB test set.
- **WBCIC-MI** (Yang et al., 2025) is a high-quality motor imagery EEG dataset comprising recordings from 62 healthy participants (ages 17–30) across three sessions. For pretraining, we incorporate the officially released preprocessed signals: 4-second trials recorded with 58 EEG channels.
- **ABIDE** is an international collaborative initiative that aggregates resting-state fMRI, structural MRI and phenotypic data collected independently across more than 24 imaging centers worldwide. It contains two large-scale collections: **ABIDE-I** (Di Martino et al., 2014), which includes 1,112 participants (ages 7–64; 539 individuals with autism spectrum disorder and 573 controls), and **ABIDE-II** (Di Martino et al., 2017), which includes 1,114 participants (521 individuals with autism spectrum disorder and 593 controls).
- **ABRIM** (Jansen et al., 2023) is a cross-sectional adult lifespan MRI collection comprising structural and functional MRI scans from 295 healthy participants (ages 18–80), along with cognitive assessments, proxy measures of cognitive reserve, and 7-day actigraphy recordings of sleep-wake rhythms. After removing corrupted and missing data, a total of 282 subjects are included in our pretraining dataset.
- **AOMIC** (Snoek et al., 2021) is one of the largest and richest open-access 3 T neuroimaging resources focused on young adults. It comprises three complementary datasets: **ID1000** (N = 928, ages 19–26), **PIOP1** (N = 216, age 18–26) and **PIOP2** (N = 226, ages 18–26), together providing 1,370 unique participants. Each sub-cohort includes high-resolution T1-weighted structural MRI, diffusion-weighted imaging, multiple resting-state runs, and an exceptionally broad battery of task-based fMRI paradigms (naturalistic movie watching, emotion processing, working memory, face recognition, cognitive conflict and response inhibition).
- **CHCP** (Ge et al., 2023) is the Chinese Human Connectome Project, comprising neuroimaging and behavioral data from 366 healthy adults living in an Eastern culture. Its acquisition protocols closely mirror the original HCP-YA, including high-resolution T1w/T2w structural MRI, resting-state and task-based fMRI (seven tasks), and high-angular-resolution diffusion MRI, as well as behavioral data based on Chinese population.
- **CoRR** (Zuo et al., 2014) is the largest publicly available test-retest resting-state fMRI consortium, aggregating data from 36 independent research groups across 18 international sites. The dataset comprises 5,093 resting-state fMRI scans from 1,629 unique participants (ages 6–88), with many individuals providing multiple sessions. This multi-site, multi-scanner design introduces natural acquisition variability highly beneficial for learning robust representations.
- **DLBS** (Park et al., 2025) is a longitudinal adult lifespan neuroimaging dataset designed to characterize brain-cognition relationships across aging. A total of 464 participants (ages 21–89 at baseline) completed the first assessment, with 338 and 224 participants returning for second and third assessment epochs, respectively, at intervals of approximately 3.5–5 years. Each epoch includes an extensive neuropsychological battery, questionnaires assessing physical health, psychosocial factors and brain health, as well as multimodal MRI acquisitions: T1-weighted structural imaging, diffusion-weighted imaging, hypercapnia imaging, arterial spin labeling and four functional MRI scans (resting-state and task-based fMRI), totaling 6,893 fMRI sessions across all visits.
- **NADR** (Spreng et al., 2022) is a multisite neuroimaging dataset designed to characterize age-related differences in brain function. It includes 301 healthy adults, comprising 181 young adults (ages 18–34) and 120 older adults (ages 60–89). Each participant underwent two 10-minute multi-echo resting-state fMRI runs and a high-resolution T1-weighted MPRAGE structural scan acquired on 3T MRI scanners across two sites.
- **Narratives** (Nastase et al., 2021) is a naturalistic paradigm dataset comprising 891 fMRI runs from 345 healthy adults (age 18–53 years) who listened to 27 different spoken stories. These stories vary widely in length, speaker, and content, together providing 4.6 hours of unique auditory narrative stimulation (43,000 words).

- **NKI-RS** (Tobe et al., 2022) is a large-scale longitudinal lifespan neuroimaging initiative comprising 1,344 participants, designed to characterize developmental and aging trajectories across the human lifespan. The dataset provides comprehensive psychiatric, medical, behavioral and cognitive phenotyping, along with multimodal brain imaging across multiple follow-up visits (resting-state fMRI, diffusion MRI, structural morphometric MRI and arterial spin labeling), genetic data and actigraphy measures.
- **Paingen placebo** (Botvinik-Nezer et al., 2024) is a large-scale, high-quality pain and placebo analgesia fMRI collection comprising 395 healthy adults (age 30–43 years). Each participant completed four fMRI runs during a well-controlled thermal pain and placebo manipulation paradigm, plus anatomical scans and field maps.
- **QTIM** (Blokland et al., 2011; Sinclair et al., 2015) is one of the largest twin neuroimaging cohorts worldwide. It comprises resting-state and task-based fMRI from 1,202 young adult twins and siblings (ages 12–30 at baseline), including a test-retest subsample (N = 78, 3.5-month interval) and longitudinal adolescent twin cohorts scanned at ages 12 and 16 (N = 88 each), with a subset rescanned four years later (N = 24 at both 12 and 16; N = 38 at 16 and 20).
- **REST-meta-MDD** (Chen et al., 2022) is a large-scale resting-state fMRI consortium for major depressive disorder (MDD), aggregating data from 25 research groups across 17 hospitals in China. It comprises 2,428 resting-state fMRI scans from 1,300 patients with MDD and 1,128 healthy controls, providing a diverse and clinically representative sample for studying MDD alterations in brain function.
- **SALD** (Wei et al., 2018) is a cross-sectional adult lifespan neuroimaging dataset comprising structural MRI and resting-state fMRI from 493 healthy adults (ages 19–80). All scans were acquired on a 3 T Siemens Trio scanner at the Brain Imaging Center of Southwest University, China.
- **SpaceTop** (Jung et al., 2025) is a landmark naturalistic and multidimensional neuroimaging dataset comprising 101 healthy young adults, each completing approximately 40 fMRI runs. It uniquely integrates a broad spectrum of experimental paradigms, including cognitive, affective, social and somatic/interoceptive tasks, together with structural T1-weighted imaging, multi-shell diffusion MRI and autonomic physiological recordings.
- **UCLA CNP** (Poldrack et al., 2016) is a publicly shared neuroimaging dataset comprising 272 adults (ages 21–50): 130 healthy controls and 142 patients (50 schizophrenia, 49 bipolar disorder, 43 ADHD). The dataset provides an extensive set of imaging modalities, including task-based fMRI across multiple cognitive domains, resting-state fMRI, structural MRI and high-angular-resolution diffusion MRI.
- **CamCAN** (Taylor et al., 2017) is a large multimodal, cross-sectional adult lifespan dataset from 656 healthy adults (ages 18–87). It includes 3T resting-state and task fMRI (movie-watching and sensorimotor task) as well as high-density MEG (306-channel Elekta Neuromag, 1,000 Hz sampling rate) during both resting state and the same sensorimotor task. For pretraining, we incorporate all available fMRI and MEG data except subjects assigned to downstream validation and test sets. This strict subject-level exclusion prevents contamination while maximizing pretraining data volume.
- **HCP Young Adult** (Van Essen et al., 2013) includes multiple 3T and 7T fMRI runs as well as MEG recordings from 1,113 young healthy adult (ages 22–35). For pretraining, we incorporate all available functional modalities: 3T resting-state and task fMRI, 7T resting-state and task fMRI and both resting-state and task MEG.
- **LEMON** (Babayan et al., 2019) is a multimodal neuroimaging dataset that includes both fMRI and EEG recordings. Participants underwent a 3T fMRI scan and a 61-channel resting-state EEG acquisition. Due to the scarcity of high-quality multimodal datasets, we also incorporate LEMON as a downstream evaluation task. To avoid contamination in downstream evaluation, subjects overlapping with the LEMON validation and test splits are excluded from the pretraining dataset.
- **MOUS** (Schoffelen et al., 2019) is a multimodal neuroimaging dataset collected from 204 healthy adults (ages 18–33). The protocol includes whole-brain fMRI and high-density 275-channel MEG acquired during a Dutch language paradigm as well as during resting state. For pretraining, we incorporate all available MEG and fMRI sessions from the MOUS cohort.
- **OMEGA** (Niso et al., 2016) is a large, open-access collection of resting-state MEG recordings led by the McConnell Brain Imaging Centre (BIC) at the Montreal Neurological Institute (MNI), McGill University, in collaboration with the Université de Montréal. It is a continuously expanding resource; for this study, we include resting-state MEG from 644 participants (444 healthy controls and 200 patients with various psychiatric conditions).

- **WAND** (McNabb et al., 2025) is a multiscale, multimodal neuroimaging dataset comprising in vivo brain data from 170 healthy adults (ages 18–63), including 3T and 7T structural and functional MRI as well as 275-channel MEG recorded at a 1,200 Hz sampling rate. We incorporate all available resting- and task-state fMRI (3 T and 7 T) and MEG data into the pretraining dataset.

### A.3. Downstream Task Datasets

- **SEED-V** (Liu et al., 2021) is an emotion recognition EEG benchmark collected from 20 participants using a 62-channel ESI NeuroScan system at a 1,000 Hz sampling rate. It includes five emotion categories (happy, sad, fear, disgust and neutral) recorded across three sessions. Each session contains 15 trials, yielding a total of 117,744 1-second samples. Following the conventional strategy, we divide the fifteen trials of each session into three equal parts (5:5:5) as the training, validation and test sets, respectively.
- **CHB-MIT** (Shoeb, 2009; Goldberger et al., 2000) is an intractable-seizure EEG database comprising recordings from 22 pediatric subjects (ages 1.5–22), acquired at 256 Hz with the international 10–20 system at Children’s Hospital Boston. For our experiments, all recordings are resampled to 200 Hz and segmented into 326,993 10-second samples. Notably, seizure events constitute only 0.68% of all samples, resulting in a severe class imbalance. We follow the conventional subject-wise split: subjects 1 to 19 for training, subjects 20, 21 for validation, and subjects 22,23 for testing.
- **TUAB** (Obeid & Picone, 2016) is a subset of the TUEG corpus, containing EEG recordings from 1,385 healthy controls (normal) and 998 subjects with a brain disorder (abnormal), totaling 2,993 sessions. After preprocessing, we obtain 409,455 10-second samples for binary classification task. The official evaluation split is used as our test set. To avoid potential data leakage effects, all subjects included in the TUAB test set are excluded from the TUEG dataset.
- **ADNI** (Jack Jr et al., 2008) is a longitudinal, multisite neuroimaging initiative that includes structural, functional and molecular imaging, along with biofluid biomarkers, cognitive assessments, genetic data and demographic information from healthy older adults, individuals with mild cognitive impairment and patients with Alzheimer’s disease (AD). For this downstream task, we incorporate resting-state fMRI data from 222 participants (110 patients with AD and 112 age- and gender-matched healthy controls), yielding a total of 508 scanning sessions. After preprocessing, a total of 618 samples are used.
- **ADHD-200** (ADHD-200-consortium, 2012) is a large-scale, multi-site benchmark for neurodevelopmental classification, comprising resting-state fMRI, anatomical MRI and phenotypic data from 926 children and adolescents (573 typically developing controls, 353 individuals with ADHD) across eight international sites. In total, participants contributed 1,369 resting-state fMRI sessions. For the downstream binary ADHD vs. control classification task, all 1,369 sessions are used after mini-preprocessing.
- **CamCAN** (Taylor et al., 2017) is a widely used benchmark for studying age-related changes in brain function, particularly in MEG. It contains both MEG and fMRI recordings from 656 healthy adults spanning the adult lifespan (ages 18–87). We use this dataset for chronological brain-age prediction under three evaluation settings: (i) unimodal resting-state fMRI (652 8min40s recordings), (ii) unimodal resting-state MEG (non-overlapping 177,044 2 second segments), and (iii) multimodal fusion of fMRI and MEG. To eliminate any risk of information leakage, all subjects included in the CamCAN validation and test splits are strictly excluded from the pretraining dataset.
- **LEMON** (Babayan et al., 2019) consists of 227 healthy participants divided into a young cohort ( $N = 153$ , age  $25.1 \pm 3.1$  years, range 20–35 years, 45 female) and an elderly cohort ( $N = 74$ , age  $67.6 \pm 4.7$  years, range 59–77 years, 37 female). For downstream age-group classification (young vs. elderly), we evaluate on three settings: (i) unimodal fMRI using 438 7.5-minute resting-state scans, (ii) unimodal EEG using non-overlapping 17,235 10-second segments, and (iii) multimodal fusion of fMRI and EEG. To prevent information leakage and ensure reliable downstream evaluation, all subjects in the LEMON validation and test splits are excluded from the pretraining dataset.

## B. Baseline Models

To compare our models with representative baselines, we include both task-specific models and recent foundation models across different modalities, as summarized in Table 6.

Task-Specific Models:

- ContraWR (Yang et al., 2023b) is a CNN-based encoder that employs contrastive learning on short-time Fourier transform (STFT) spectrograms for automated EEG sleep staging.
- CNN-Transformer (Peh et al., 2022) combines convolutional neural networks with transformer layers and employs a belief-matching loss to enable automated detection of EEG artifacts.
- FFCL (Li et al., 2022) employs two independent branches that fuse multilevel spatial–temporal features, integrating CNN and LSTM architectures for EEG decoding.
- ST-Transformer (Song et al., 2021) is a transformer-based architecture that leverages spatial–temporal attention mechanisms to capture both spatial dependencies and temporal dynamics in EEG signals for decoding tasks.

Foundation Models:

- LaBraM (Jiang et al., 2024) is a unified EEG foundation model that enables cross-dataset generalization by segmenting raw EEG signals into channel-wise patches for transformer-based representation learning.
- CBraMod (Wang et al., 2024a) is an EEG foundation model that employs a criss-cross attention mechanism to jointly capture frequency domain and temporal features for self-supervised representation learning.
- BrainHarmonix-F (Dong et al., 2025) is the fMRI branch of the BrainHarmonix, a multimodal brain foundation model designed to process and integrate both structural and functional MRI data.

Table 6. **Overview of baseline models.** We categorize baselines into task-specific models (trained from scratch) and foundation models (pretrained). **Params** denotes parameter count in millions (M); **GFLOPs** measures computational cost per inference sample.

Model	Params (M)	GFLOPs	Architecture	Pretraining Modality
<i>Task-Specific Models (Trained from scratch)</i>				
ContraWR	1.57	0.28	CNN	✗
CNN-Transformer	3.16	0.33	CNN + Transformer	✗
FFCL	2.47	0.96	CNN + LSTM	✗
ST-Transformer	3.43	0.22	Transformer	✗
<i>Foundation Models (Pretrained)</i>				
LaBraM	5.82	2.70	Transformer	EEG
CBraMod	4.88	1.86	Criss-Cross Transformer	EEG
BrainHarmonix-F	85.25	1450.00	Vision Transformer	fMRI

The high computational cost of BrainHarmonix-F (1,450 GFLOPs) primarily derives from two factors: its support for long-range inputs exceeding 7k tokens and its large parameter count.

### C. Modality Importance Analysis

To quantify the contribution of each modality to overall model performance, we introduce a *Modality Importance Score*. This score is derived from the modality ablation results and measures the relative performance degradation on downstream tasks when a specific modality is removed during pretraining.

Because downstream tasks use evaluation metrics with different units and scales, we normalize the impact using the relative percentage drop in performance. Formally, the importance score of modality  $M_i$  on dataset  $D_j$  is defined as:

$$I_{M_i, D_j} = \frac{\mathcal{P}_{\text{all}}^{(ij)} - \mathcal{P}_{\text{ablated}}^{(ij)}}{\mathcal{P}_{\text{all}}^{(ij)}} \times 100\%$$

where  $\mathcal{P}_{\text{all}}^{(ij)}$  denotes the performance of the full Brain-OF model on dataset  $D_j$ , and  $\mathcal{P}_{\text{ablated}}^{(ij)}$  denotes the performance when modality  $M_i$  is excluded from pretraining. A positive value indicates that modality  $M_i$  contributes constructively to task  $D_j$ . Notably, for lower-is-better metrics (e.g., MAE),  $I_{M_i, D_j}$  is sign-flipped to preserve a consistent contribution direction.

As shown in Figure 3(a), the local importance heatmap reveals strong cross-modal dependencies across tasks. Figure 3(b) further aggregates these scores to obtain the *Global Modality Importance*. Overall, EEG contributes the most to general performance (score 3.87), followed by fMRI (3.54) and MEG (3.43), highlighting the complementary and non-dominant roles of all three modalities within Brain-OF.

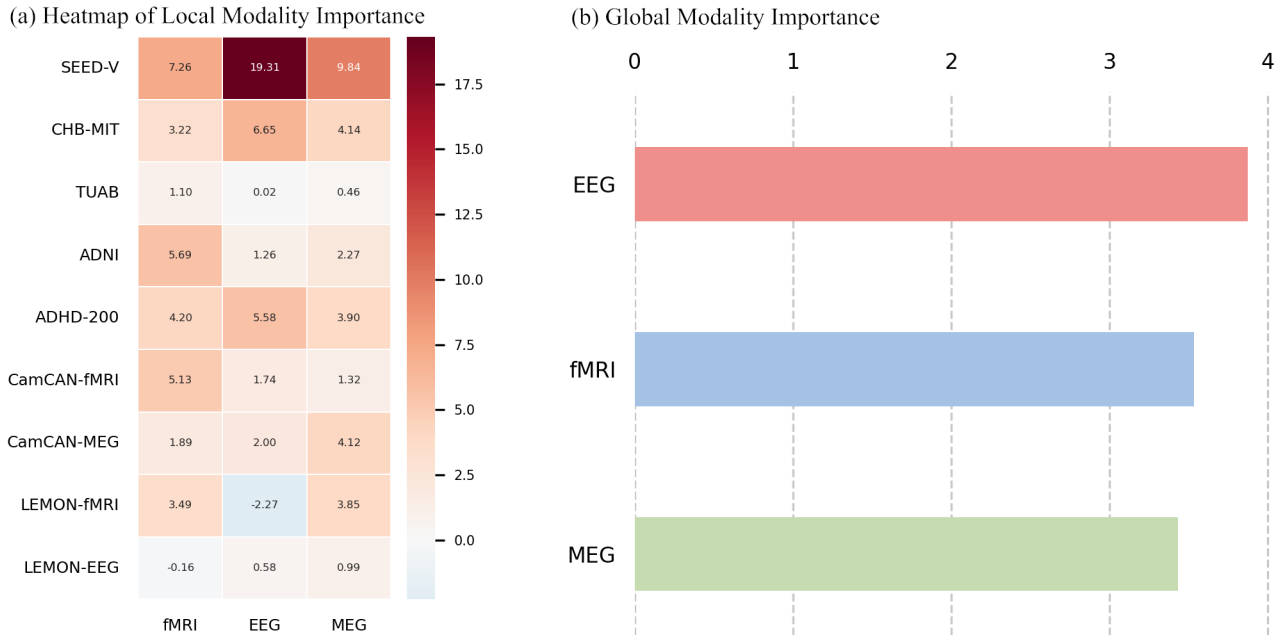


Figure 3. **Modality Importance Analysis.** (a) *Local Modality Importance.* Heatmap showing the relative performance drop (%) on each downstream dataset when a specific modality (fMRI, EEG, or MEG) is removed during pretraining. Higher values indicate stronger reliance on that modality. (b) *Global Modality Importance.* Importance scores aggregated across all downstream tasks, illustrating that EEG and fMRI contribute most to the overall generalization capability of Brain-OF, while MEG provides complementary support.

## D. Ablation Study of Mask Ratios in the MTFM

To investigate the impact of the mask ratio in the MTFM, we evaluate ratios from 0.4 to 0.9 using the Brain-OF Base model on three representative downstream datasets: TUAB (EEG) for abnormal detection, ADNI (fMRI) for Alzheimer’s diagnosis, and CamCAN (MEG) for brain age prediction. We adopt a symmetric masking strategy where the temporal and frequency mask ratios are set to the same value. The results are summarized in Table 7. Performance drops sharply at a low mask ratio of 0.4 across all modalities and metrics, so we do not explore ratios below this threshold. For TUAB and ADNI, a ratio of 0.7 yields the strongest overall results (e.g., 81.88% BAC on TUAB, 68.23% BAC on ADNI), though 0.8 performs comparably on ADNI (74.53% AUROC). In contrast, ratios of 0.6 and 0.5 are superior on CamCAN (e.g., 8.83 MAE at 0.6), but underperform on fMRI. Balancing these trade-offs, we select 0.7 as the final mask ratio for MTFM. Interestingly, different modalities exhibit preferences for distinct optimal ranges: fMRI favors higher ratios (0.7–0.8) whereas EEG and MEG benefit from moderate ones (0.5–0.7), revealing modality-specific sensitivities in self-supervised learning.

Table 7. Performance comparison across different mask ratios in the MTFM.

Mask Ratios	TUAB (EEG)			ADNI (fMRI)			CamCAN (MEG)		
	BAC(%) $\uparrow$	AUC-PR(%) $\uparrow$	AUROC(%) $\uparrow$	BAC(%) $\uparrow$	AUC-PR(%) $\uparrow$	AUROC(%) $\uparrow$	MAE $\downarrow$	R2(%) $\uparrow$	MAPE(%) $\downarrow$
$\mathcal{N}(0.4, 0.05^2)$	81.02 $\pm$ 0.12	87.17 $\pm$ 0.09	88.67 $\pm$ 0.06	61.10 $\pm$ 2.57	69.84 $\pm$ 2.36	67.54 $\pm$ 2.47	11.93 $\pm$ 0.38	32.70 $\pm$ 3.92	23.25 $\pm$ 0.77
$\mathcal{N}(0.5, 0.05^2)$	81.74 $\pm$ 0.21	87.59 $\pm$ 0.13	89.29 $\pm$ 0.19	65.01 $\pm$ 2.91	75.24 $\pm$ 2.28	71.42 $\pm$ 2.84	8.92 $\pm$ 0.18	<b>58.19</b> $\pm$ 1.71	17.00 $\pm$ 0.31
$\mathcal{N}(0.6, 0.05^2)$	81.82 $\pm$ 0.31	87.64 $\pm$ 0.20	<b>89.45</b> $\pm$ 0.27	63.74 $\pm$ 2.76	72.87 $\pm$ 3.12	70.85 $\pm$ 3.31	<b>8.83</b> $\pm$ 0.19	57.02 $\pm$ 1.94	<b>16.50</b> $\pm$ 0.48
$\mathcal{N}(0.7, 0.05^2)$	<b>81.88</b> $\pm$ 0.17	<b>87.69</b> $\pm$ 0.11	89.26 $\pm$ 0.09	<b>68.23</b> $\pm$ 2.07	76.23 $\pm$ 1.87	73.27 $\pm$ 0.71	8.99 $\pm$ 0.14	56.19 $\pm$ 1.84	16.92 $\pm$ 0.30
$\mathcal{N}(0.8, 0.05^2)$	81.51 $\pm$ 0.09	87.46 $\pm$ 0.06	89.14 $\pm$ 0.09	67.86 $\pm$ 2.62	<b>76.77</b> $\pm$ 3.17	<b>74.53</b> $\pm$ 4.71	9.45 $\pm$ 0.40	53.27 $\pm$ 3.62	18.06 $\pm$ 0.51
$\mathcal{N}(0.9, 0.05^2)$	81.26 $\pm$ 0.25	87.31 $\pm$ 0.16	88.76 $\pm$ 0.35	64.76 $\pm$ 3.78	71.61 $\pm$ 3.31	69.25 $\pm$ 2.23	10.39 $\pm$ 0.32	44.38 $\pm$ 2.75	19.94 $\pm$ 0.66

The results presented above are obtained with the Brain-OF Base.

## E. Ablation Study of Router Bias Update Rate $\gamma$

To examine the sensitivity of Brain-OF to the router bias update rate  $\gamma$  during pretraining, we conduct an ablation study over a range of values from  $10^{-5}$  to  $10^{-2}$ . Each pretrained model is subsequently fully finetuned and evaluated on three representative downstream tasks: TUAB (EEG), ADNI (fMRI) and CamCAN (MEG).

As illustrated in Figure 4, a consistent optimal configuration emerges across all modalities. In particular,  $\gamma = 10^{-3}$  achieves the highest Balanced Accuracy on EEG and fMRI tasks and the lowest Mean Absolute Error on MEG. Larger values

(e.g.,  $10^{-2}$ ) lead to noticeable performance degradation, likely due to overly aggressive bias updates that destabilize expert routing and impair specialization. In contrast, smaller values ( $10^{-5}$ ) fail to sufficiently update the router bias, limiting the effectiveness of load balancing.

Interestingly, we observe a different preference during the finetuning stage. While  $\gamma = 10^{-3}$  is crucial for effective pretraining, substantially smaller update rates (e.g.,  $\gamma = 10^{-5}$ ) generally yield improved stability and performance during downstream finetuning, preserving the specialized knowledge acquired during pretraining.

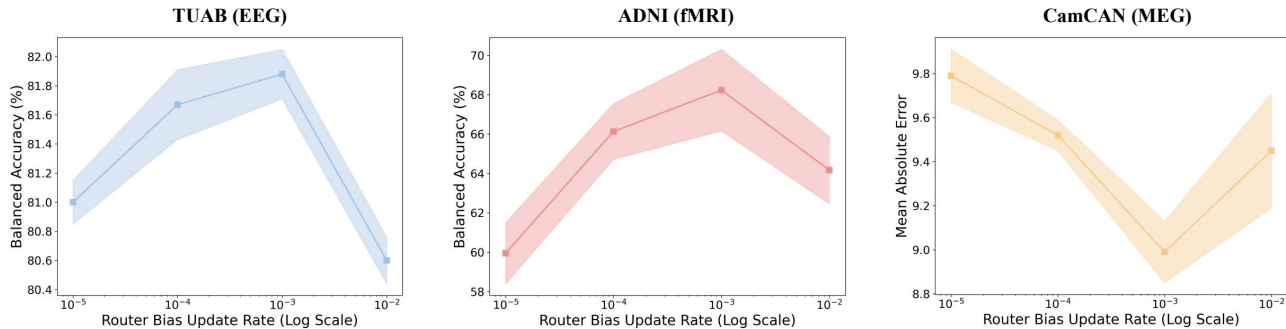


Figure 4. The impact of the router bias update rate  $\gamma$  during pretraining. The performances are evaluated on downstream tasks across three modalities.

## F. Visualization of Reconstruction

We visualize the reconstruction quality of Brain-OF Huge to assess the effectiveness of the proposed Masked Temporal-Frequency Modeling (MTFM) objective across fMRI, EEG, and MEG. Beyond simple waveform reconstruction, we examine whether the model preserves critical high-order features. As shown in Figure 5, Brain-OF achieves high-fidelity reconstruction with effective noise suppression. For EEG, reconstructed signals closely match the original temporal dynamics while preserving dominant spectral bursts. In fMRI, functional connectivity derived from the original and reconstructed BOLD signals show that the complex inter-regional correlation structure is well preserved. For MEG, reconstructed topomaps accurately recover localized scalp-level magnetic field patterns despite signal sparsity. Overall, these results indicate that Brain-OF learns meaningful spatiotemporal and spectral generative structure rather than memorizing raw inputs.

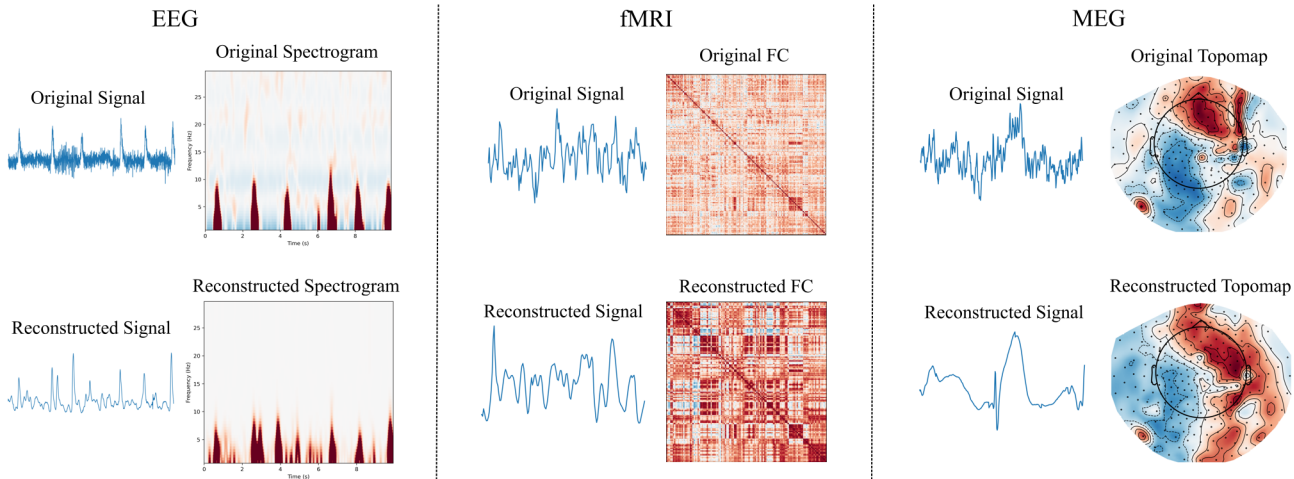


Figure 5. Qualitative visualization of signal reconstruction across fMRI, EEG and MEG.

## G. Hyperparameter Configurations

In this section, we provide the detailed hyperparameter configurations in the Brain-OF pretraining, as well as the optimization settings for downstream tasks. All models were implemented in PyTorch and trained on NVIDIA A100 GPUs using automatic mixed precision.

## G.1. Pretraining Settings

Table 8. Hyperparameters for pretraining Brain-OF.

Hyperparameters		Brain-OF Base	Brain-OF Large	Brain-OF Huge
	Model Size	47.5M	331M	1.7B
	Activated Parameters	21.5M	150M	500M
	Patch size		64	
	Max sequence length		2048	
	Semantic space size		128	
	Padding token		Full zero	
Brain Signal Encoder	Input dimension	{1, 4, 4}	{1, 8, 8}	{1, 12, 12}
	Output dimension	{4, 4, 4}	{8, 8, 8}	{12, 12, 12}
	Kernel size		{3, 3, 3}	
	Stride		{1, 1, 1}	
	Padding		{1, 1, 1}	
Brain-OF	ARNES layer	4	4	6
	Backbone layer	12	24	36
	Attention head	4	8	12
	Hidden dimension	256	512	768
	Routed expert	8	16	28
	Activated expert	2	4	4
	Shared expert		1	
Pretraining settings	Epochs		150	
	Global batch size	7,168 (224×32 GPUs)	7,040 (80×88 GPUs)	7,168 (32×224 GPUs)
	Optimizer		AdamW	
	Adam $\beta$		(0.9, 0.95)	
	Peak learning rate		3e-3	
	Warmup learning rate		3e-5	
	Router bias update rate		1e-3	
	Learning rate scheduler		Cosine	
	Warmup epochs		8	
	Weight decay		0.05	
	Gradient clipping		5.0	
	Mask ratio		$\mathcal{N}(0.7, 0.05^2)$	
	Layer scale init	1e-4	1e-5	1e-6

## G.2. Finetuning Settings on Downstream Tasks

For downstream tasks, Brain-OF is fully finetuned with a lightweight task-specific linear head following global average pooling. We employ cross-entropy loss for classification tasks and mean squared error loss for regression tasks. Optimization is performed using AdamW with  $\beta = (0.9, 0.99)$  and a cosine learning rate scheduler. Detailed finetuning hyperparameter configurations for different model variants are provided in Table 9, Table 10 and Table 11.

Table 9. Hyperparameters for downstream finetuning (Brain-OF Base).

Datasets	Global bsz	Epochs	Warmup epochs	Lr	Warmup lr	Weight decay	Drop out	Drop path
SEED-V	1,024	50	5	1e-4	1e-6	5.0	0.0	0.0
CHB-MIT	1,024	50	5	3e-5	3e-7	0.1	0.0	0.1
TUAB	1,024	50	5	7e-6	7e-8	0.1	0.0	0.0
ADNI	32	50	5	1.5e-4	1.5e-6	0.1	0.1	0.0
ADHD-200	32	50	5	3e-5	3e-7	0.01	0.1	0.0
CamCAN-fMRI	32	100	5	7.5e-4	7.5e-6	0.1	0.1	0.0
CamCAN-MEG	1,024	50	5	1e-4	1e-6	5e-4	0.0	0.0
CamCAN-MM	512	50	5	2e-4	2e-6	0.1	0.0	0.2
LEMON-fMRI	32	100	5	2e-4	2e-6	0.1	0.1	0.1
LEMON-EEG	512	50	5	1.5e-5	1.5e-7	0.1	0.0	0.0
LEMON-MM	512	50	5	4e-5	4e-7	0.1	0.0	0.3

MM (Multimodal): Indicates finetuning Brain-OF on multimodal scenarios. Specifically, CamCAN comprises paired fMRI and MEG, while LEMON comprises paired fMRI and EEG.

Table 10. Hyperparameters for downstream finetuning (Brain-OF Large).

Datasets	Global bsz	Epochs	Warmup epochs	Lr	Warmup lr	Weight decay	Drop out	Drop path
SEED-V	1,024	50	5	4e-4	4e-6	5.0	0.0	0.1
CHB-MIT	1,024	50	5	3e-5	3e-7	0.5	0.0	0.1
TUAB	1,024	50	5	3e-5	3e-7	0.1	0.0	0.3
ADNI	32	50	5	1e-4	1e-6	0.1	0.0	0.3
ADHD-200	32	50	5	4e-5	4e-7	0.01	0.1	0.2
CamCAN-fMRI	32	100	5	3e-3	3e-5	0.1	0.1	0.1
CamCAN-MEG	1,024	50	5	6e-4	6e-6	0.1	0.0	0.3
CamCAN-MM	512	50	5	8e-5	8e-7	0.05	0.0	0.2
LEMON-fMRI	32	100	5	3e-4	3e-6	0.1	0.0	0.1
LEMON-EEG	512	50	5	6e-4	6e-6	0.1	0.0	0.1
LEMON-MM	512	50	5	4e-4	4e-6	0.1	0.0	0.1

MM (Multimodal): Indicates finetuning Brain-OF on multimodal scenarios. Specifically, CamCAN comprises paired fMRI and MEG, while LEMON comprises paired fMRI and EEG.

Table 11. Hyperparameters for downstream finetuning (Brain-OF Huge).

Datasets	Global bsz	Epochs	Warmup epochs	Lr	Warmup lr	Weight decay	Drop out	Drop path
SEED-V	1,024	50	5	1e-4	1e-6	5.0	0.0	0.1
CHB-MIT	1,024	50	5	1e-4	1e-6	0.1	0.0	0.1
TUAB	1,024	50	5	7e-6	7e-8	0.1	0.0	0.1
ADNI	32	50	5	3e-4	3e-6	0.1	0.0	0.1
ADHD-200	32	50	5	1e-4	1e-6	0.1	0.0	0.3
CamCAN-fMRI	32	100	5	5e-3	5e-5	0.1	0.0	0.1
CamCAN-MEG	1,024	50	5	4e-4	4e-6	0.1	0.0	0.3
CamCAN-MM	512	50	5	1e-3	1e-4	0.1	0.0	0.3
LEMON-fMRI	32	100	5	5e-4	5e-6	0.1	0.001	0.1
LEMON-EEG	512	50	5	1.5e-4	1.5e-6	0.1	0.0	0.1
LEMON-MM	512	50	5	4e-4	4e-6	0.1	0.0	0.1

MM (Multimodal): Indicates finetuning Brain-OF on multimodal scenarios. Specifically, CamCAN comprises paired fMRI and MEG, while LEMON comprises paired fMRI and EEG.

## H. Efficiency Analysis

We evaluate the computational efficiency of Brain-OF across three model scales: Base, Large and Huge. Table 12 summarizes the parameter counts, training resources and inference latency.

**Model Scaling and Training Cost.** Brain-OF employs a Sparse Mixture of Experts architecture, which decouples the total parameter count from the computational cost per forward pass. Although Brain-OF Huge contains 1.7B parameters, only approximately 500M parameters (29%) are activated per token. This sparsity enables efficient scaling: while the total parameter count increases by  $35\times$  from Base (47.5M) to Huge (1.7B), the number of active parameters grows by only  $\sim 23\times$ . Pretraining the Huge variant required 153 hours on 224 NVIDIA A100 GPUs.

**Inference Latency and Throughput.** Inference latency is measured on a single NVIDIA A100 GPU using BF16 precision, with a sequence length of 2,048 tokens and a batch size of 16. The average *per-sample* latency remains low: 5.5 ms for Base, 11.1 ms for Large, and 18.6 ms for Huge. This corresponds to a throughput of 181.8 samples/s for the Base model, indicating that Brain-OF remains suitable for real-time despite its large-scale architecture. Notably, the efficiency is further enhanced by ARNESS, which compresses high-dimensional brain signals into a compact semantic representation, significantly reducing the effective token length and computational burden.

Table 12. Efficiency analysis across model variants. **Active Params** denotes the number of parameters used per forward pass (due to sparse MoE). **Inference Latency** is reported for a batch size of 16 with sequence length 2,048 on a single A100 GPU.

Model Variants	Total	Active	Comp.	Pretraining Cost		Inference (Batch=16)	
	Params	Params	GFLOPs	Time	# GPUs	Latency	Throughput
Brain-OF Base	47.5M	21.5M	11.29	71h 50m	32	88 ms	181.8 samples/s
Brain-OF Large	331M	150M	61.01	82h 06m	88	178 ms	89.9 samples/s
Brain-OF Huge	1.7B	500M	178.19	153h 03m	224	297 ms	53.8 samples/s

## I. Representation Visualizations on Downstream Datasets

To qualitatively assess the learned representations, we employ t-SNE (Maaten & Hinton, 2008) to visualize the feature embeddings generated by finetuned Brain-OF across three downstream datasets. Figure 6 illustrates the evolution of representations from raw input features (Column 1) to embeddings learned by Brain-OF Base, Large and Huge (Columns 2–4). The first two rows correspond to classification tasks on TUAB (EEG) and ADNI (fMRI). In the raw feature space, samples from different classes (e.g., Normal vs. Abnormal, Healthy Control vs. Alzheimer’s Disease) are heavily entangled. As model capacity increases from Base to Huge, a clear trend emerges: class-specific clusters become progressively more compact and better separated. This confirms that scaling the model capacity directly enhances its ability to extract discriminative, class-specific representations. The third row visualizes the regression task on CamCAN (MEG), where color gradients indicate chronological age. Unlike the unstructured scatter of the raw data, the Brain-OF embeddings organize into a coherent, continuous manifold where age varies smoothly across the representation distribution. This structure suggests that Brain-OF captures meaningful biological variation associated with aging, rather than merely fitting discrete targets. Overall, these visualizations demonstrate that scaling Brain-OF enhances both class separability in classification tasks and structural coherence in regression settings, validating the effectiveness of large-scale omnifunctional pretraining.

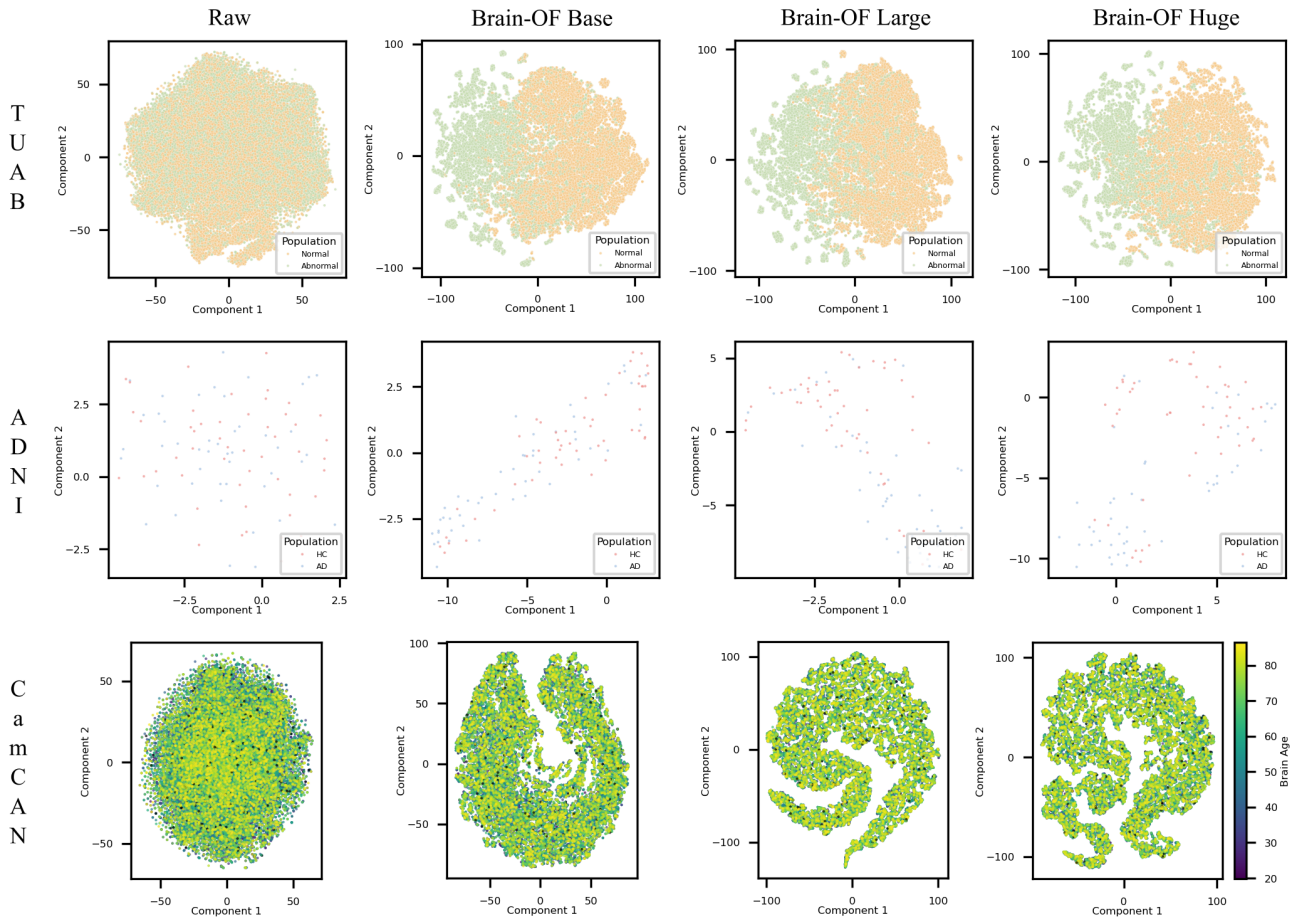


Figure 6. **t-SNE visualization of learned representations across model scales.** Comparison of raw input features (Left) with representations from Brain-OF Base, Large and Huge (Right). Rows correspond to different modalities and tasks: **Top:** TUAB (EEG, binary classification); **Middle:** ADNI (fMRI, binary classification); **Bottom:** CamCAN (MEG, age regression). As model size increases, the representations exhibit clearer class separation (Top/Middle) and a more structured continuous manifold for regression (Bottom), demonstrating the benefits of scaling.

## J. Ablation Study on Key Components

To verify the contribution of key architectural components, we conduct ablation studies on the Sparse MoE and DINT attention mechanism. Specifically, we pretrain two variants: (i) replacing Sparse MoE with a dense Feed-Forward Network (FFN), and (ii) substituting DINT attention with vanilla self-attention. As shown in Table 13, replacing Sparse MoE with a dense FFN results in the largest performance degradation across all tasks, with particularly severe drops on fMRI tasks. This suggests that a shared dense parameter space struggles to disentangle heterogeneous modality semantics, as the larger EEG/MEG corpora may dominate gradient updates in the dense model, hindering learning of subtle features from the smaller fMRI corpus. In contrast, Sparse MoE enables expert specialization, mitigating negative transfer and preserving performance even on under-represented modalities. Replacing DINT attention with vanilla self-attention also leads to consistent but smaller performance declines (e.g., SEED-V Cohen’s  $\kappa$  drops from 23.98% to 22.82%). This indicates that standard attention is susceptible to the low signal-to-noise ratio of neural recordings, attending to irrelevant fluctuations rather than meaningful patterns. DINT alleviates this issue by suppressing irrelevant context and emphasizing salient signals. Overall, these ablations demonstrate that Sparse MoE and DINT attention are both crucial for handling semantic heterogeneity and noise in brain signals.

Table 13. Ablation analysis of key components.

Method	SEED-V	TUAB	ADNI	ADHD-200	CamCAN
	EEG	EEG	fMRI	fMRI	MEG
	Kappa(%) $\uparrow$	BAC(%) $\uparrow$	BAC(%) $\uparrow$	BAC(%) $\uparrow$	MAE $\downarrow$
<b>Brain-OF (Base)</b>	<b>23.98<math>\pm</math>0.29</b>	<b>81.88 <math>\pm</math>0.17</b>	<b>68.23<math>\pm</math>2.07</b>	62.57 $\pm$ 1.19	<b>8.99<math>\pm</math>0.14</b>
w/ Dense FFN	20.86 $\pm$ 0.28	81.86 $\pm$ 0.08	64.60 $\pm$ 3.32	59.10 $\pm$ 1.80	9.78 $\pm$ 0.27
w/ Vanilla Attn.	22.82 $\pm$ 0.38	81.85 $\pm$ 0.09	64.32 $\pm$ 2.82	<b>62.82<math>\pm</math>1.76</b>	9.50 $\pm$ 0.53

## K. Label Efficiency and Low-Resource Analysis

To evaluate Brain-OF’s robustness under data-scarce conditions, we assess the Brain-OF Base using progressively smaller fractions (10%–100%) of the downstream training data. We consider two representative tasks: abnormality detection on TUAB (EEG) and brain-age prediction on CamCAN (MEG). As illustrated in Figure 7, Brain-OF exhibits strong label efficiency across both tasks. For TUAB (left), the model achieves over 81.5% balanced accuracy using only 30% of the labeled data, nearly approaching the full-data performance of 81.88%. For CamCAN (right), the mean absolute error consistently decreases as more data becomes available, yet the model maintains competitive accuracy even in low-resource settings (e.g., 30% training data). These results indicate that the rich, generalizable representations learned during large-scale multimodal pretraining reduce the dependency on large labeled downstream datasets. Brain-OF thus offers promising potential for low-resource neuroimaging scenarios, where annotated data is often limited or expensive to obtain.

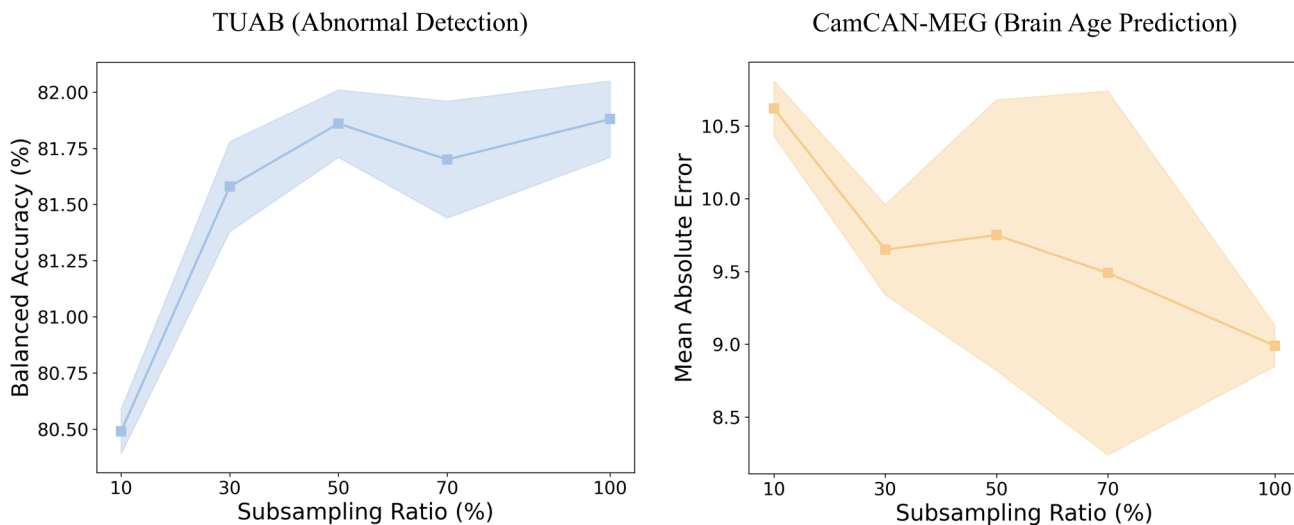


Figure 7. **Label efficiency of Brain-OF under limited supervision.** Brain-OF Base is evaluated across varying training data fractions (10%, 30%, 50%, 70%, 100%). Shaded regions denote standard deviation across five random seeds. Brain-OF achieves strong performance even with limited labeled data, highlighting the effectiveness of heterogeneous multimodal pretraining for low-resource settings.

## L. Limitations and Future Work

Although we curate one of the largest neuroimaging corpora to date, which spans over 40 datasets across fMRI, EEG and MEG, the overall data scale remains orders of magnitude smaller than that of foundation models in natural language processing or computer vision. Moreover, the pretraining corpus exhibits notable modality imbalance, with fMRI samples being considerably scarcer than EEG and MEG recordings. Future iterations of Brain-OF may address these challenges by incorporating additional modalities such as fNIRS and PET, and by extending the framework to support more general multivariate time series.

Currently, Brain-OF employs a relatively straightforward multimodal fusion strategy. While effective, this approach may not fully capture complex and nonlinear cross-modal interactions. Future work could explore more expressive fusion mechanisms, such as adaptive gating strategies or dedicated cross-modal attention modules, to better model fine-grained inter-modality dependencies.

In this work, downstream performance is evaluated using full finetuning, which offers strong representational capacity but incurs substantial computational and memory costs. Future research will investigate parameter-efficient fine-tuning (PEFT) techniques, such as LoRA or adapter-based methods, to reduce the computational burden while maintaining performance.